LITHOS xxx (xxxx) 106591

Contents lists available at ScienceDirect

LITHOS

journal homepage: www.elsevier.com/locate/lithos

Geochemical variability among stratiform chromitites and ultramafic rocks from Western Makran, South Iran

Hadi Shafaii Moghadam [a, b, *], Shoji Arai [c], William L. Griffin [b], Mohamed Z. Khedr [d], Emilio Saccani [e], Hadrien Henry [b], Suzanne Y. O'Reilly [b], Ghasem Ghorbani [a]

[a] School of Earth Sciences, Damghan University, Damghan 36716-41167, Iran
[b] CCFS and GEMOC ARC National Key Centre, Macquarie University, NSW 2109, Australia
[c] Faculty of Science, Kanazawa University, Ishikawa 920-1192, Japan
[d] Department of Geology, Kafrelsheikh University, Egypt
[e] Dipartimento di Fisica e Scienze della Terra, Università di Ferrara, Ferrara 44122, Italy

ARTICLE INFO

Keywords:
Stratiform chromitites
Ultramafic rocks
Geochemical variations
Makran
Iran

ABSTRACT

The geochemical compositions of minerals from the Moho transition zone of ophiolites potentially can help to understand the magmatic evolution of the ophiolites, and subsequent mantle-melt interactions. The Jurassic-Late Cretaceous Makran ophiolite of south Iran comprises one of the most extensive tracts of oceanic crust which were scraped off and preserved in an accretionary complex. The Makran ophiolite records traces of MORB-OIB-type magmatism during the Jurassic, but mostly supra-subduction zone magmatic activity during the Late Cretaceous. Despite a few geochemical studies on the crustal rocks, the nature and geochemical signatures of the mantle rocks from this ophiolite remain controversial. The Sorkhband mantle-crust transition zone underlying crustal cumulates in the western Makran consists of stratiform chromitites, harzburgites, chromite-rich dunites and dunites, with crosscutting dikes of olivine websterite and olivine clinopyroxenite. Major- and trace-element compositions of clinopyroxene grains in olivine websterite and clinopyroxenite dikes indicate crystallization from melts similar to boninites and low-Ti fore-arc basalts. Spinel compositions in olivine websterite and clinopyroxenite dikes suggest crystal fractionation from boninitic or high- Mg# magmas have played a major role in the genesis these rocks.

We propose a two-stage model for the formation of the Sorkhband dunites including (1) supra-subduction zone-related melt infiltrates through harzburgites in the mantle-crust transition zone to dissolve peridotite orthopyroxene and leave dunites with high forsterite-NiO olivines, and (2) boninitic melts accumulate and react with surrounding harzburgites to crystallize cumulate dunites with low-Mg# olivine and high-Ti spinels. We conclude that there have been temporal changes in the composition of mantle melts in the fore-arc mantle section of the Makran ophiolite during the initial subduction of the Neotethyan ocean beneath the Lut block during the Late Cretaceous.

1. Introduction

Ophiolites are widely used to reconstruct the geochemical and magmatic processes responsible for building the oceanic lithosphere in different geodynamic settings. Recent studies show that most ophiolites form in supra-subduction zones (-SSZ), some in back-arcs but mostly in fore-arcs (Stern and Gerya, 2017). The magmatic rocks comprising the crustal sections of ophiolites from supra-subduction zones are geochemically variable, in both space and time. For example, the magmatic rocks can change temporally from fore-arc basalts-Medium-Ti basalts to boninites from subduction initiation to arc infancy, and then to calc-alkaline rocks during arc maturity, as reported in the Izu-Bonin-Mariana subduction system as well as from the Neotethyan SSZ-related ophiolites (e.g., Saccani et al., 2018b; Saccani and Tassinari, 2015; Stern and Gerya, 2017). Mantle peridotites can also be used to understand the magmatic evolution of the ophiolites, the processes that were involved during magma generation and subsequent mantle-melt interactions (e.g., Arai et al., 2006; Choi et al., 2008; Jean et al., 2010). Detailed studies of fore-arc peridotites have been obstructed by the difficulty in obtaining samples, aside from those drilled or dredged from

* Corresponding author at: School of Earth Sciences, Damghan University, Damghan 36716-41167, Iran.
E-mail address: hadishafaii@yahoo.com (H.S. Moghadam).

https://doi.org/10.1016/j.lithos.2021.106591
Received 29 October 2021; Received in revised form 30 December 2021; Accepted 30 December 2021
0024-4937/

subduction zones, e.g., in the Izu-Bonin-Mariana subduction system (Parkinson and Pearce, 1998a). Most geochemical variations can be observed in the mantle-crust dunitic transition zone (or MOHO transition zone) of ophiolites such as Oman (e.g., Rospabe et al., 2017; Rospabe et al., 2018). The mantle-crust transition zone, which is located beneath the crustal ultramafic-mafic cumulates, is a link between the mantle upwelling and magma delivery and is dominantly composed of dunites with various types of melt segregations such as gabbros, wehrlites, pyroxenites and chromitites. The reaction between melts and mantle harzburgite, which may play an important role in the formation of the MOHO transition zone, is very complicated. It includes processes such as melt-orthopyroxene reaction, olivine crystallization/accumulation, harzburgite partial melting as well as intense percolation of magmas with different geochemical signatures (Meshi et al., 2010).

Layered harzburgites, dunites and pyroxenites accompany the stratiform chromitites from the dunitic transition zone (DTZ) of ophiolites, such as Oman and Mediterranean ophiolites. Stratiform chromitites are mostly interlayered with dunites and harzburgites or may alternate with pyroxenites and gabbros. Stratiform chromitites together with depleted harzburgites and dunites are common in the western Makran ophiolite of south Iran, especially in the Sorkhband-Rudan area between Minab and Manujan (Fig. 1). This ophiolite records a phase of subduction infancy during the Late Cretaceous. To better understand the geochemical variabilities in the mantle section of SSZ-ophiolites, we have sampled stratiform chromitites and their associated peridotites, olivine clinopyroxenites and websterites from the Sorkhband ultramafic complex in the western Makran ophiolite. This is the first systematic geochemical study on the Makran ultramafic rocks and stratiform chromitites. This paper aims to understand the genesis of dunites, stratiform chromitites and olivine clinopyroxenites - websterites in the mantle-crust transition zone and to investigate how these different rocks are related to geochemical variations among different sectors of the supra-subduction zone mantle wedge.

2. Geological background

The Iranian Makran is a well-known accretionary complex developed above a subduction zone during north-ward subduction of Neotethyan oceanic lithosphere beneath the Lut block (e.g., Esmaeili et al., 2019; Saccani et al., 2018a). The Makran comprises a region of about 200 km wide in south Iran between the Jazmurian depression (to the North) and the Gulf of Oman (to the South) (Supplementary Fig. S1). The Makran accretionary complex extends for 450 km, from southeast Iran to southwest Pakistan. To the north, in the Chagai and Ras Koh Mountain ranges of Pakistan and the Bazman and Taftan regions of Iran, there are rock sequences that represent the associated magmatic arc. The Makran accretionary complex contains remnants of Jurassic-Cretaceous off-scraped oceanic lithosphere and associated sedimentary rocks as well as relicts of a mature arc (e.g., Hunziker et al., 2015; McCall, 1997). Exhumed high-pressure ophiolites including lawsonite-bearing blueschists (Deyadar complex) are common in the Makran accretionary complex, and Rb-Sr isochron ages show that the HP-LT metamorphism occurred in Late Cretaceous (Bröcker et al., 2021). In addition, the Makran accretionary complex includes a thick sequence of Mesozoic to Cenozoic flysch-type sediments, which accumulated during the growth stage of the Makran accretionary complex.

There are three important zones in the Iranian Makran, from south to north: (1) the Makran accretionary complex which formed through the subduction of Neotethyan oceanic lithosphere beneath the Lut block, (2) the Jazmurian depression, a sediment-filled Mesozoic back-arc basin, and (3) Cenozoic volcanic and plutonic rocks of andesitic to rhyolitic composition which reflect arc magmatism related to the Makran subduction system. Ophiolites are abundant in the Makran accretionary complex and can be divided into two parts (Fig. 1): (1) Southern Makran ophiolitic mélange (the Jurassic-early Paleocene Makran ophiolitic belt of Mccall (2002) and (2) Northern Makran ophiolites including several ophiolitic units. Eocene to Pliocene sequences of calcareous and turbiditic flysch, evaporites, reef limestone, gypsiferous mudstone, deltaic sandstone and estuarine conglomerate are also common and their presence in the southernmost Makran accretionary complex testifies to the southward growth of the Makran complex during Cenozoic time.

2.1. Northern Makran ophiolite belt

There are five distinct ophiolitic slices/complexes in this belt (Fig. 1), comprising from west to east: (a) the Band-e-Zeyarat/Dare Anar complex, including Early Cretaceous pelagic sediments and a magmatic suite including cumulate gabbros, high-level isotropic gabbros (with amphibole ^{40}Ar-^{39}Ar ages of 142.9 ± 3.5 to 140.7 ± 2.2 Ma; Ghazi et

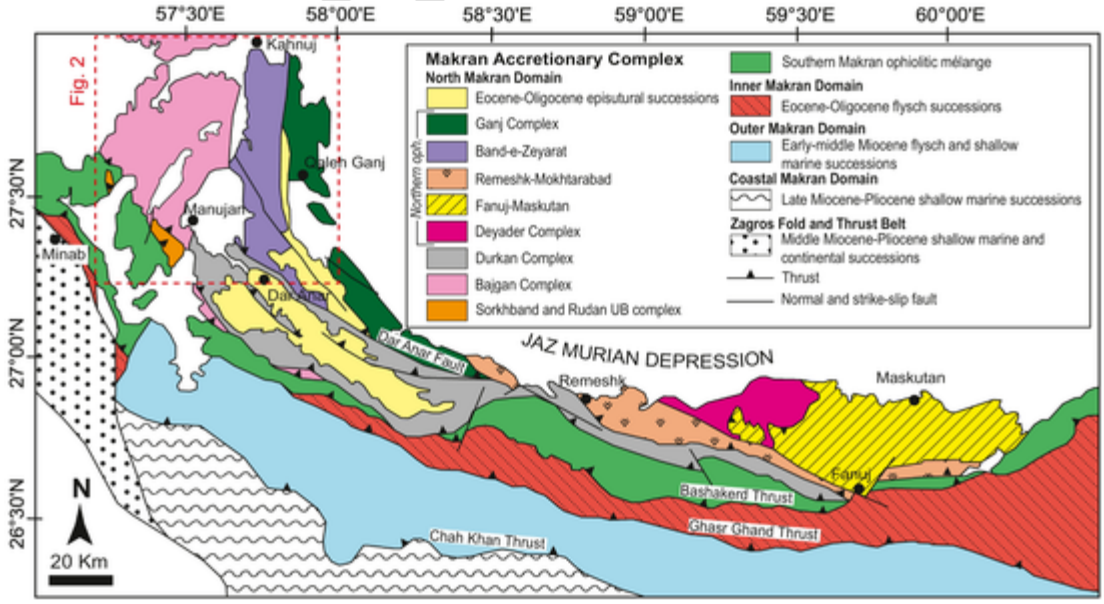

Fig. 1. Detailed tectonic map of the Makran accretionary complex, showing the main magmatic-metamorphic complexes of the North Makran Domain, as well as the Inner, Outer and Coastal Makran tectono-sedimentary units (modified after Barbero et al., 2020).

al., 2004), trondhjemites, a diabasic sheeted dike complex, and pillow lavas, all with tholeiitic affinities; (b) the Cretaceous Ganj complex, which is a calc-alkaline sequence thrust on top of the Band-e-Zeyarat/Dare Anar complex; (c) the Rameshk-Mokhtarabad complex, which is a Late Jurassic-Early Cretaceous to Early Paleocene ophiolitic slice, consisting of fragmented ultramafic-mafic cumulates, high-level gabbros, trondhjemites (with zircon U-Pb ages of 145 and 111 Ma; Hunziker et al., 2015), a sheeted dike complex, pillow lavas and pelagic sediments; (d) the Fanuj-Maskutan complex, composed of ultramafic-mafic rocks, upper crustal N-MORB-like pillow lavas, and associated Early Cretaceous pelagic sediments to terrigenous turbidites, overlain by Late Cretaceous-Paleocene shallow-water sediments and supra-subduction zone- (SSZ-) related lavas (Burg, 2018; Hunziker et al., 2015); and (e) the Deyadar lawsonite-bearing blueschists (Hunziker et al., 2017).

The Ganj complex is a > 2000 m thick sequence consisting of a dike swarm and volcano-sedimentary rocks with Turonian-Coniacian microfossil ages. Volcanic rocks and dikes have intermediate to acidic compositions with minor basalts, all with calc-alkaline to island-arc tholeiitic compositions. The Ganj complex is interpreted as remnants of a Turonian-Coniacian volcanic arc that was most likely forming in a relatively shallow marine environment in an extensional intra-arc setting (Barbero et al., 2020).

2.2. Bajgan-Durkan complex

The Bajgan-Durkan complex was previously assumed to represent the remnants of a continental ribbon located between the northern and southern Makran ophiolites (e.g., Mccall, 2002). The Jurassic magmatic rocks within the Bajgan-Durkan complex were also assumed to be produced by arc magmatism, although a rift origin has recently been proposed (Hunziker et al., 2015). The Bajgan-Durkan complex comprises Late Jurassic to Early Cretaceous and Paleocene meta-ophiolites and related pelagic meta-sediments that were affected by low- to medium-pressure/low-temperature metamorphism within a Late Cretaceous subduction system (Barbero, 2021; Pandolfi et al., 2021). Recent studies show that the Bajgan-Durkan complex consists of Early Cretaceous to Paleocene metapelites, carbonates and volcanic successions which appear to be remnants of oceanic seamounts (Barbero et al., 2021a; Barbero et al., 2021b; Pandolfi et al., 2021); there is no clear evidence for considering it as a continental ribbon.

2.3. Sothern Makran ophiolitic mélange

This mélange is located south of the Bajgan-Durkan complex and consists of tectonic slices of serpentinites, pillow lavas, pelagic limestones, radiolarites and distal turbidites. It is suggested to have formed in the trench of a North-dipping subduction zone by scraping off fragments of the downgoing plate during Late Cretaceous to Early Paleocene time (Burg, 2018; Mccall, 2002). There are no radiometric ages on the southern ophiolitic mélange; biomicrites intercalated with pillow lavas contain Campanian-Maastrichtian microfaunas, although there are also Cenomanian, Turonian, Coniacian and Santonian microfossils (Mccall, 2002). The radiolarites associated with pillow lavas and pelagic limestones range from Pliensbachian (Jurassic) to Coniacian. The ophiolitic mélange zone at the contact with the Bajgan complex includes two ultramafic complexes, Sorkhband and Rudan, which both contain chromitite ore deposits.

3. Sorkhband ultramafic complex

The samples for this study were collected mainly from the Sorkhband ultramafic complex (Fig. 1). Due to the extensive mining in this area, systematic sampling from lower parts to the upper parts is difficult and sometimes impossible, but our samples come from localities in which the contacts between units are preserved. This complex contains poorly- to well-layered dunites, harzburgites and chromitites (± pyroxenites). The Sorkhband complex is in fault contact with Bajgan Early Cretaceous-Paleocene and/or Late Cretaceous metamorphic rocks (Figs. 2, 3a), including pelitic to psammitic and calcareous schists, recrystallized limestones and meta-volcanic successions represented by greenschists and amphibolites (Barbero et al., 2021a; Barbero et al., 2021b). Metagabbros, meta-peridotites and felsic plutonic rocks are also present. The Sorkhband ultramafic complex contains mostly depleted harzburgites, with interlayered dunites and chromitites and rare clinopyroxenites. Thick dunitic layers with disseminated chromite separate the layered chromitite-dunite-clinopyroxenite sequences (Fig. 3b). Stratiform chromitites with interlayered dunites are common. Chromitite layers vary from centimetres to tens of centimetres thick and are rhythmically recurrent with centimetric to metric dunitic interlayers (Fig. 3c-d). The textures of chromitites change from disseminated in thick dunitic layers to cumulate in chromite-rich dunites and to massive in chromitite layers. Stratiform chromitites are affected by *syn*-magmatic faults and folds (Fig. 3e), which have led to the displacement and/or folding of the chromitite layers, probably during the subsolidus cooling stage. Dunites, chromitites and depleted harzburgites are crosscut by later serpentine, magnesite and/or chromium-rich garnet (uvarovite) veins. Abundant dikes of olivine clinopyroxenite to olivine websterite randomly crosscut dunites and harzburgites (Fig. 3f). Most dikes occur separately but some dikes crosscut one another. There is no systematic temporal relationship between olivine websterite and clinopyroxenite dikes. Harzburgites (±dunites) locally show traces of magmatic impregnation by basaltic melts– represented by clinopyroxene cumulates– at the contact and/or near the olivine clinopyroxenite and websterite dikes. Xenoliths of host harzburgites can be observed in some clinopyroxenite and websterite dikes. Plagioclase-bearing clinopyroxenite and websterite dikes/dikelets are very rare and crosscut harzburgites and/or olivine websterite dikes. The Sorkhband ultramafic sequence is overlain by an eroded leucogabbroic-anorthosite layered sequence <100 m thick. At the contact between ultramafic rocks and leucogabbroic-anorthosite layered rocks, pegmatite gabbros-leucogabbros, flaser gabbros and gabbronorites are injected into ultramafic rocks as dikes to small plutons. The contacts of these late-stage intrusions with the ultramafic rocks are faulted and fragmented, but in some places, the intrusive contacts are sharp and clear.

4. Samples

We have sampled harzburgites, dunites, stratiform chromitites and clinopyroxenites-websterites from the Sorkhband complex for geochemical and textural studies. Below, we describe the mineralogical characteristics of these rocks.

4.1. Harzburgites

Harzburgites are poor in clinopyroxene (1–2%) with orthopyroxene ranging from 20 to 30%. Orthopyroxene occurs as coarse-grained porphyroclasts (3-4 mm). These rocks contain serpentinized olivine (with 40–50% serpentine) and fine-to coarse-grained (~0.1 to 3–4 mm) spinels. Irregular-shaped clinopyroxenes are also present in some harzburgites and seem to be residual clinopyroxene (Fig. 4a). The shape of these clinopyroxenes and their occurrence between olivine crystals suggests that these clinopyroxenes are different than those formed by exsolution of the primary high-temperature orthopyroxenes.

4.2. Melt-impregnated harzburgites

In these rocks, coarse-grained crystals of clinopyroxene are set between the serpentinized olivines. Orthopyroxene is also present as large (3-4 mm) porphyroclasts whereas spinel is fine-grained (~1 mm).

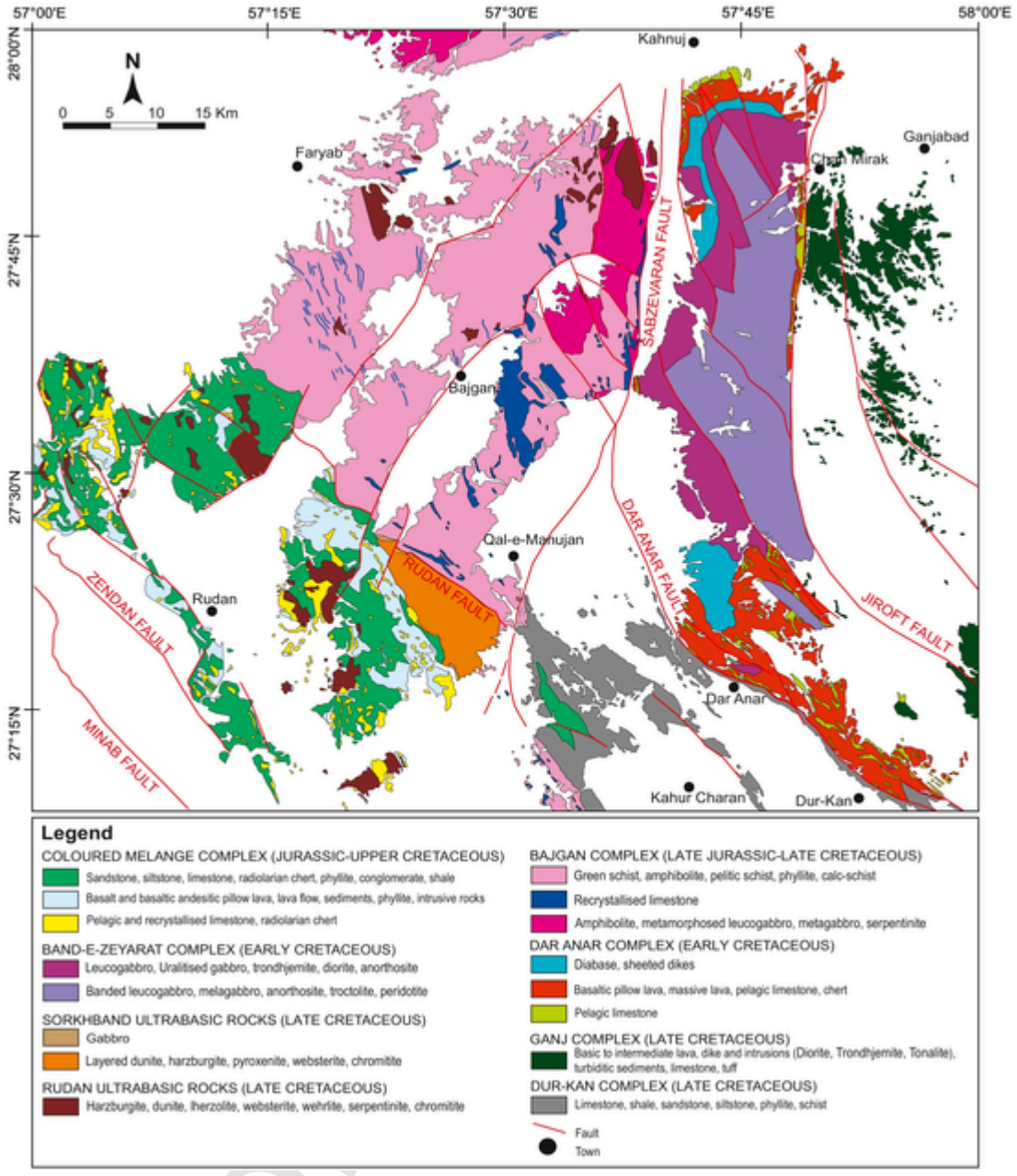

Fig. 2. Geological map of the Minab area with emphasis on the Sorkhband ultramafic rocks (modified after Samimi Namin and et.al., 1983).

4.3. Dunites

Dunites from the Sorkhband complex are highly serpentinized (40–50% to 70%) and contain olivine, spinel and rare residual clinopyroxene crystals (Fig. 4b). Dunites contain euhedral to subhedral, fine-grained to very fine-grained (< 0.2 mm) spinels. Some dunites (impregnated dunites) contain rare clinopyroxene crystals, along with brownish irregular-shaped spinels. The impregnating clinopyroxenes are coarse-grained, crosscut the olivine aggregates and are found near the olivine websterite and clinopyroxenite dikes, whereas residual clinopyroxenes are tiny and irregular and occur along olivine grain boundaries.

4.4. Chromite-rich dunites

These rocks have coarse-grained, kinked olivine porphyroclasts with 30–40% coarse-grained (> 5 mm) chromite crystals (Supplementary Fig. S2a) and are 50–60% to 80% serpentinized. The chromite grains occur as scattered polygonal crystals in contact with serpentinized cumulate olivines, similar to the chromite-rich dunites at the crust-mantle boundary.

4.5. Chromitites

Massive (stratiform) chromitites contain > 70% chromite grains in a serpentinized matrix (70–80%) and/or chromites occur between partly serpentinized olivines. Cr-rich garnet (uvarovite) occurs as veins in the massive chromitites.

4.6. Olivine websterites and olivine clinopyroxenites

Olivine websterites from the Sorkhband complex mostly show coarse-grained cumulate texture, containing large (3-4 mm) to fine-grained (~1 mm) clinopyroxenes. The large clinopyroxenes are surrounded by fine-grained orthopyroxene crystals. In some olivine web-

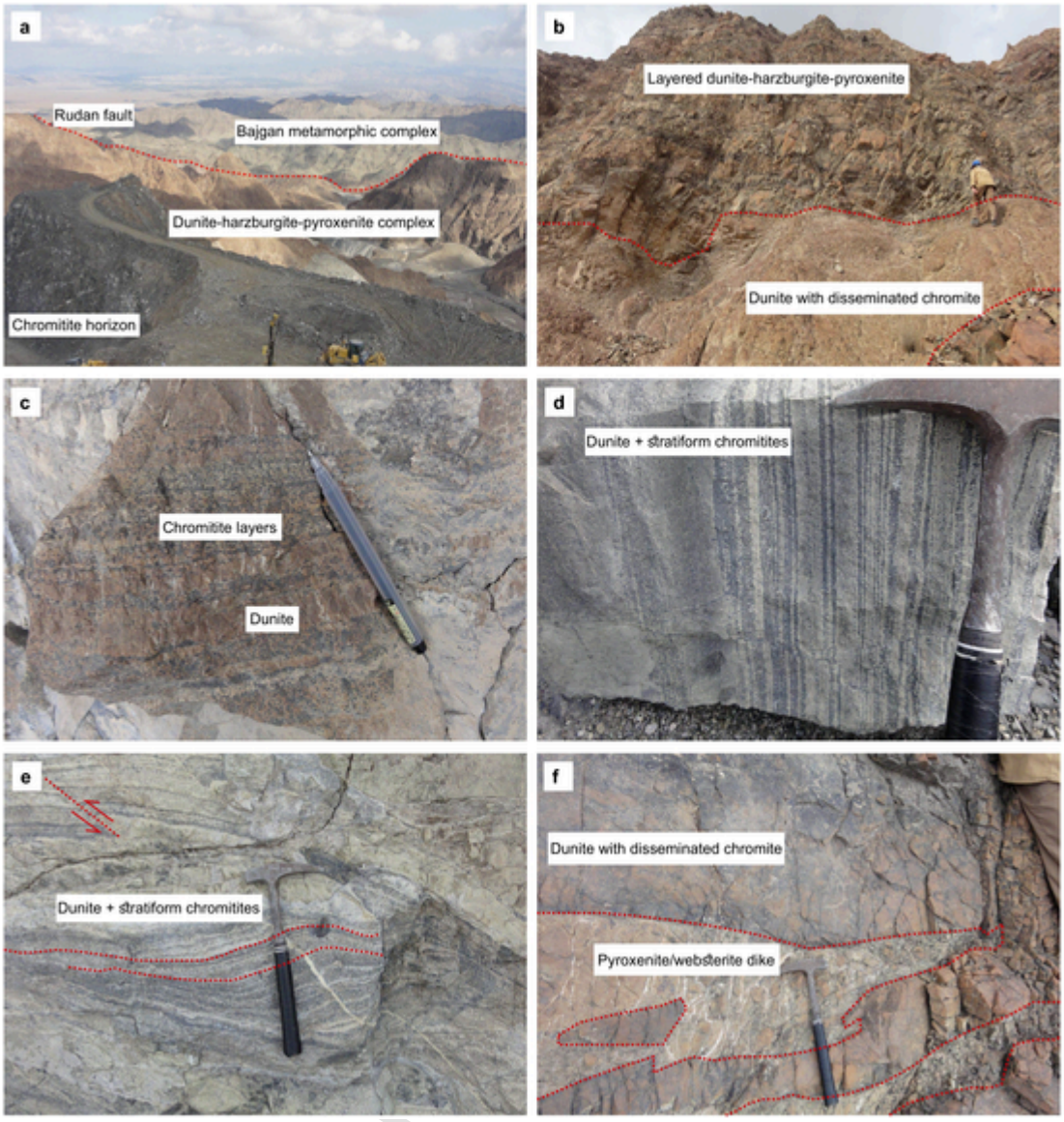

Fig. 3. Field photos from the Sorkhband ultramafic complex. a- Stratiform chromitites (chromite horizon) and Sorkhband dunite-harzburgite-pyroxenite complex at the contact with the Bajgan metamorphic rocks. b- thick dunitic layers intercalated with layered dunite-harzburgite and pyroxenites sequences. c and d- Stratiform chromitites and centimetric to metric serpentinized dunite layers. e- Syn-magmatic faults and folds displaced and bent the layers of stratiform chromitites. f- Intrusive dikes with olivine websterite and clinopyroxenite composition crosscut the Sorkhband harzburgites and dunites.

sterites, orthopyroxene is interstitial to the large clinopyroxenes, producing heteradcumulate textures (Fig. 4c). Olivine grains are also present, along with orthopyroxene and fine-grained clinopyroxenes, between the large clinopyroxenes, showing heteradcumulate (Fig. 4d) or poikilitic adcumulate (Fig. 4e) textures. Fine-grained to tiny spinel grains (<1 mm) also occur between other magmatic phases in these rocks. Some olivine websterites comprise cumulus crystals of clinopyroxene and orthopyroxene with olivine and amphibole as intercumulus phases (Fig. 4f-g).

Olivine clinopyroxenites are similar to olivine websterites but show more clinopyroxene and less intercumulus orthopyroxene and olivine. These rocks are mostly coarse-grained with a granular texture. Some olivine clinopyroxenites contain very large clinopyroxene crystals (> 5 mm) with rare orthopyroxene grains between clinopyroxenes and have a polygonal protogranular texture. Some clinopyroxenes show exsolution lamellae.

4.7. Plagioclase-bearing clinopyroxenites

In addition to the olivine websterites and olivine clinopyroxenite dikes, there are some plagioclase-bearing clinopyroxenite dikelets in the Sorkhband dunites and harzburgites. These rocks have large clinopyroxenes with intercumulus plagioclase crystals that now are altered to epidote, clay minerals and hydrogrossular (Fig. 4h). Fine-grained, euhedral crystal of spinels are also common in these rocks.

5. Results

5.1. Mineral deformation

To understand and to quantify the deformation style (*if any*) of the Sorkhband chromitites and ultramafic rocks, we selected six samples of dunites, chromitites, olivine websterites and olivine clinopyroxenites for the electron backscattered diffraction analysis. Below, we describe the results of the EBSD studies. The crystallographic preferred orientations of olivine, clinopyroxene, orthopyroxene and amphibole in

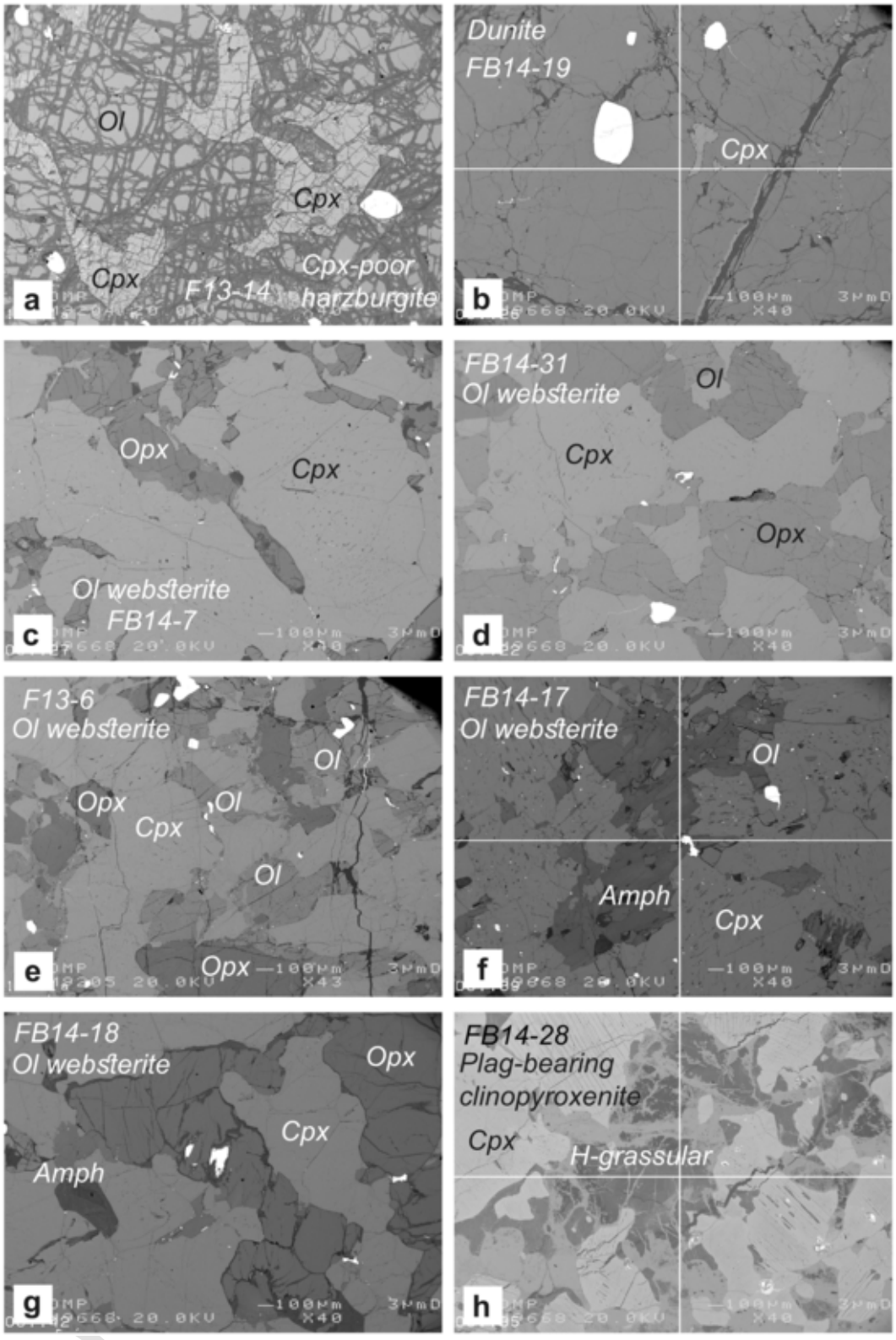

Fig. 4. Electron back-scattered images of the Sorkhband ultramafic rocks. a- Residual clinopyroxene in depleted harzburgites. b- Residual, fine-grained clinopyroxene in dunites. c- Large clinopyroxene phenocrysts and late-stage crystallized interstitial orthopyroxenes in olivine websterites. d- Cumulate crystals of clinopyroxene, orthopyroxene and olivine in olivine websterites. e- Fine-grained orthopyroxene and olivine in large crystals of clinopyroxenes forming the poikilitic adcumulate texture. f- Large clinopyroxene phenocrysts, amphibole crystals and fine-grained, interstitial olivines in olivine websterites. g- Large clinopyroxene cumulate crystals, intercumulus orthopyroxene and amphibole in olivine websterites. h- Altered plagioclase (into hydrogrossular) and clinopyroxene in plagioclase-bearing clinopyroxenites.

dunites, chromitites, olivine websterites and clinopyroxenites from the Sorkhband complex are shown in Supplementary Fig. S3.

5.1.1. Dunite sample FB14–19

Olivine in this sample has a bimodal grain size distribution. Large grains (~2 mm) are predominant and coexist with smaller grains (~250-500 μm). This sample displays complex curvilinear grain boundaries, undulous extinction and kinking in both grain-size population. A shape-preferred orientation is visible with the flattening and elongation of some olivine grains from the large grain size population. The important and striking internal deformation recorded suggest that this sample has not experienced an important recovery episode. Analysis of olivine subgrains indicates the activation of the [100](010) slip system in some olivine grains. The deformation markers, SPO (Fig. 5a) and the well-marked fabric suggest that this sample recorded plastic deformation in the dislocation creep regime, probably at high temperatures and low stress (Jung and Karato, 2001).

5.1.2. Dunite sample F13–5

This sample is coarse-grained with a unimodal grain size distribution (~1–2 mm). Grains have either complex shapes or display a weak shape-preferred orientation marked by an elongation or flattening. Grain boundaries between olivine crystals are mostly curvilinear with 120° triple junctions. Olivine shows kink bands with development of subgrains which are less pronounced than in sample FB14–19 (Fig. 5b). The olivine fabric is very well-defined, not random and has [100] axis point maximum corresponding to the elongation direction of olivine crystals in the section. In addition, both [010] and [001] axes define girdles perpendicular to the [100] axis. The fabric pattern would be best described as a D-type olivine fabric.

The curved grain boundaries of the olivine-olivine contacts suggest recrystallisation by grain-boundary migration. This, together with the relatively low internal deformation and the 120° triple junction all point toward the recording of an episode of textural recovery.

5.1.3. Chromitite sample FB14–4

This sample contains abundant chromite (~800 μm) with interstitial olivine grains (~250 μm). Olivine can form elongated clusters and mark a planar feature. Most chromite grains have subgrains close to the contacts with other chromite grains but some subgrains cut across them entirely (Fig. 5c). Coarse-grained and deformed chromite grains are sometimes present next to smaller and relatively more equilibrated ones, suggesting a deformation episode and possibly incipient recrystallization of the chromite. Olivine is also deformed internally with subgrain and undulose extinction. Olivine CPO shows a concentration of [010] axes and a girdle of [100] at 90° to [010]. [010] axes being perpendicular to the planar feature defined by interstitial olivines, we interpret it as a [010]-fibre fabric.

5.1.4. Olivine websterite sample F13–7

This sample occurs as a dike cross-cutting the harzburgites and dunites. However, it shows no obvious deformation criteria in the field, such as folding, foliation etc. This sample is granular with a mostly unimodal mineral distribution for both clinopyroxene and orthopyroxene (~1–2 mm, Fig. 5d). Still, rare smaller clinopyroxene grains (~250-500 μm) are observed scattered in the sample. Grain boundaries are straight to curvilinear for same phases contacts and are curved between different phases. The 120° contact angle are also common for same-phase triple junction. Grains are internally equilibrated, although scarce subgrains in clinopyroxene and orthopyroxene are sometimes visible. Our data show that clinopyroxene and orthopyroxene fabrics are random. Our observations point toward the annealing of the texture and static recrystallisation. The random CPO and the lack of internal deformation in the grains suggest that this sample recorded little to no plastic deformation.

5.1.5. Olivine websterite sample FB14–7

Sample FB14–7 has a bimodal grain-size distribution. Clinopyroxene makes up for the coarse-grained (~1–2 mm) fraction and most of the volume of this sample. Smaller olivine, clinopyroxene and orthopyroxene grains (~250-500 μm) are found interstitially. Grain boundaries

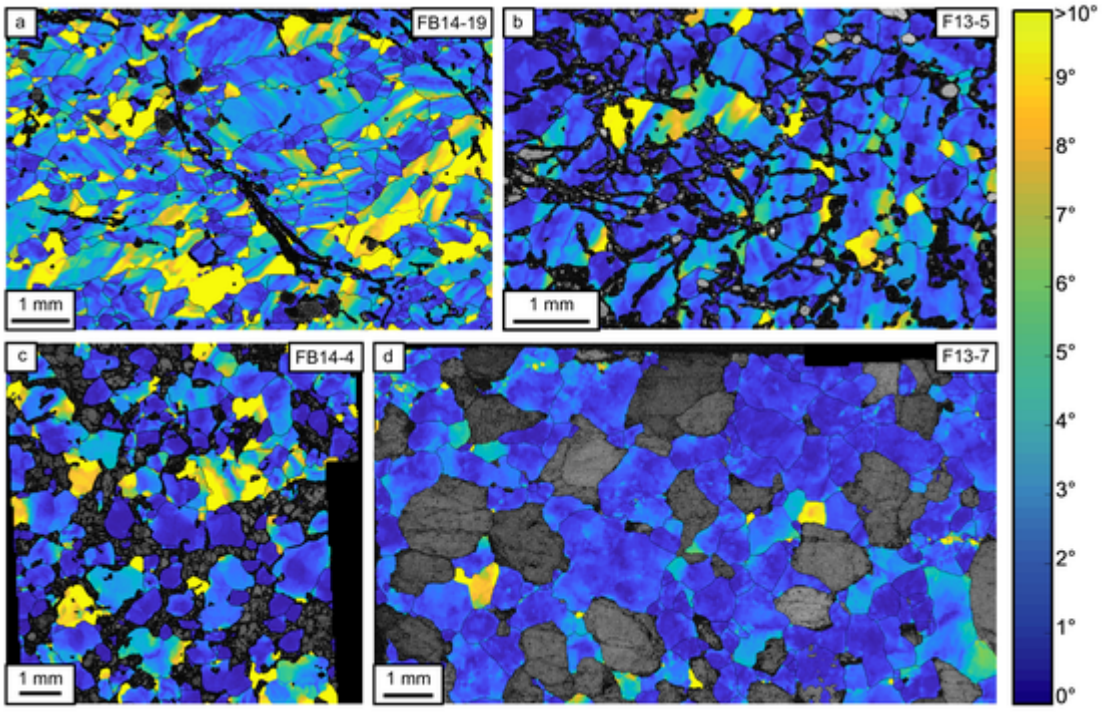

Fig. 5. Electron backscattered diffraction images of: dunites a, b- (samples F13–5 and FB14–19), c- stratiform chromitite (samples FB14–4) and d- olivine websterite (F13–7).

between similar phases are mostly straight while grains boundaries between two different phases are best described as curvilinear. Triple contact from grains with the same phase are observed to be 120°. In each phase, internal strain markers such as subgrains or undulose extinction are present. They appear mostly in the coarse-grained fraction and become rare in the fine-grained fraction. Olivine presents a weak fabric with a cluster of [010] axis and a girdle for [100] axis. Clinopyroxene fabric is also weak and presents a cluster of [100] axis. Because of the small M- and J-indices of the olivine and clinopyroxene CPO, we will not interpret this sample's fabric. However, based on the textural observations, sample FB14–7 seems to have recorded a weak plastic deformation episode (in the form of internal deformation of the minerals) and did not experience any textural recovery.

5.1.6. Olivine clinopyroxenite sample FB14–33

This sample contains coarse-grained clinopyroxenes, coexisting with smaller interstitial ones. Olivine and orthopyroxene are found as interstitial single grains or aggregates. Clinopyroxenes have straight grain boundaries with other clinopyroxenes and curved boundaries at the contact with other phases. Rare clinopyroxene subgrains are visible at high angle contacts between clinopyroxenes. Some interstitial orthopyroxene and olivine grains show kink bands, but the majority are free of internal deformation. The CPO of clinopyroxene, olivine and orthopyroxene do show clusters with similar azimuths for the [010] and [001] axes. Our observations for sample FB14–33 show that it has reached an advanced state of textural equilibrium with a rare internal deformation. The combination of a non-random CPO and the highly equilibrated texture could indicate either (1) textural recovery after a plastic deformation episode or (2) remnant of magmatic-driven arrangement of the crystals.

5.2. Major-element compositions

To understand the geochemical signatures of mineral phases from the Sorkhband chromitites and ultramafic rocks, we have analyzed major elements in the mineral phases. Below, we describe the results of the geochemical analyses.

5.2.1. Olivine

Olivine in the Sorkhband ultramafic rocks has variable composition. The forsterite content of olivine grains from dunites and clinopyroxene-bearing dunites (impregnated dunites) varies from 88.1 to 95.1, with NiO contents varying from 0.13 to 0.5 wt%. The NiO and forsterite content of olivine show a positive but non-linear correlation (Fig. 6). Some dunites such as sample F13–20 contain both refractory ($Fo_{91.4}$) and less refractory and probably impregnated ($Fo_{88.4}$) olivines, although there is no means for distinguishing refractory from non-refractory (or possibly impregnated) olivines in thin sections. This sample lacks any modal trace of melt impregnation, such as the presence of clinopyroxene, but also contains both Al- and Cr-rich spinels (see next section). Dunite sample FB14–19 contains less refractory olivine ($Fo_{88.1–88.9}$), but also minor impregnating clinopyroxene.

Olivine in chromite-rich dunites is highly refractory with forsterite contents of 94.9 to 97.3 (Fig. 6) and NiO abundances between 0.32 and 0.71 wt%. Forsterite contents in stratiform chromite bands range from 93.6 to 97.7 with NiO contents of 0.36–0.96 wt%. Harzburgite olivine is $Fo_{84.9–88.7}$ with NiO contents of 0.15 to 0.20 wt%, except for sample F13–9 which has higher contents of forsterite (92.4) and NiO (0.96 wt%). In addition, impregnated harzburgites have olivine with $Fo_{85.2–85.7}$ and NiO contents of 0.12–0.16 wt%. Olivine clinopyroxenites and olivine websterites have olivine with $Fo_{86.3–87.1}$ and $Fo_{83.7–89.9}$, respectively. NiO contents are 0.09 to 0.19 wt% in olivine clinopyroxenites and 0.06 to 0.26 wt% in olivine websterites.

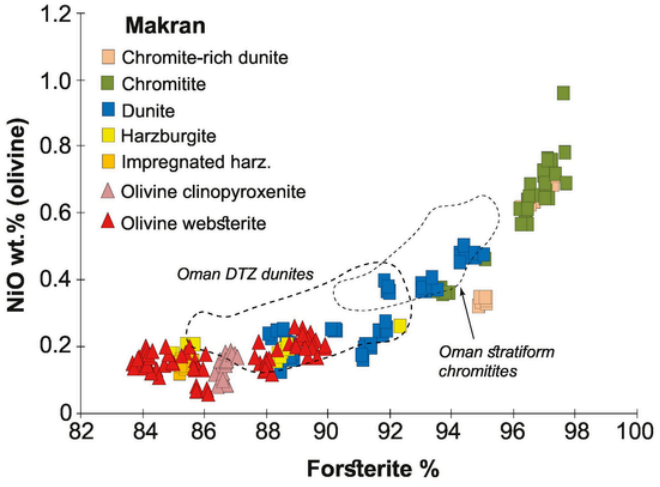

Fig. 6. Forsterite and NiO content of olivine from different rocks units of the Sorkhband ultramafic complex. For comparison, we have also shown the composition of olivine from stratiform chromitites and dunites from Oman mantle-crust or dunitic transition zone (data for Oman rocks are from Rospabé et al., 2019).

5.2.2. Spinel (chromite)

Spinels in Sorkhband dunites and impregnated dunites have very variable composition: Cr# (Cr/Cr + Al) = 0.60 to 0.83 and Mg# (Mg/Mg + Fe^{+2}) = 0.32 to 0.64, with TiO_2 contents ranging from 0.09 to 0.37 wt%. Sample F13–20 contains both Cr- rich and rather Al-rich spinels with Cr# between 0.60 and 0.72. There are no large differences between Al-rich and Cr-rich varieties in terms of Fe^{+3} and TiO_2 (Fig. 7). Chromite-rich dunites contain spinel with Cr# = 0.82–0.84, TiO_2 = 0.09–0.15 wt% and Mg# = 0.58–0.65, while chromite grains in chromitites have high Cr# = 0.76–0.83 and Mg# = 0.58–0.74, but TiO_2 of 0.07 to 0.25 wt%. High-TiO_2 spinels (TiO_2 ~ 0.25 wt%) have slightly higher Fe^{+3}# (Fe^{+3}/Fe^{+3} + Al + Cr) (~0.06 compared with other spinels with Fe^{+3}# = 0.04–0.05). Spinels in harzburgites have Cr# and Mg# ranging from 0.61 to 0.81 and 0.31 to 0.53, respectively, and TiO_2 and Fe^{+3}# in the ranges of 0.11–0.43 wt% and 0.04–0.11. Spinel in impregnated harzburgites is Al-rich (Fig. 7), with Cr# = 0.47–0.50 and Mg# = 0.39–0.43, and high TiO_2 content (0.28–0.42 wt%). Spinel Cr# and Mg# values in olivine clinopyroxenites range from 0.32–0.42 and 0.33–0.63 respectively, with TiO_2 contents of 0.04 to 0.22 wt%. Olivine websterite spinels have very variable composition with Cr# = 0.33–0.84, Mg# = 0.23–0.66, Fe^{+3}# = 0.02–0.23, and TiO_2 = 0.1–0.4 wt% (see Fig. 7). Samples with Fe^{+3}# > 0.10 have TiO_2 > 0.19 wt%. Ranges in spinel Cr# can be found both between different samples, and within samples, e.g., sample F13–31 has spinels with Cr# = 0.33–0.34 to 0.83–0.84 and sample FB14–7 has spinels with Cr# = 0.61–0.64 and 0.79.

5.2.3. Orthopyroxene

There are some tiny crystals of orthopyroxene in Sorkhband chromite-rich dunites and their Mg# and Al_2O_3 composition vary from 0.85 to 0.86 and 2.29 to 2.47 wt%, respectively, with Cr# = 0.08–0.12 and TiO_2 = 0.04–0.06 wt% (Fig. 8). Orthopyroxenes in Sorkhband olivine clinopyroxenites and olivine websterites have variable Mg# (0.85–0.91), Cr# (0.06–0.21), Al_2O_3 (0.36–2.23 wt%), TiO_2 (<0.08 wt%) and Na_2O (<0.03 wt%) (Fig. 8).

5.2.4. Clinopyroxene

There are tiny crystals of clinopyroxene in dunites and chromite-rich dunites. Clinopyroxene in chromite-rich dunites has Mg# = 0.89, Cr# = 0.15–0.16, Al_2O_3 = 2.3–2.7 wt%, Na_2O = 0.15–0.22 wt%, and TiO_2 = 0.09–0.13 wt% (Fig. 9). Dunites have residual clinopyroxene

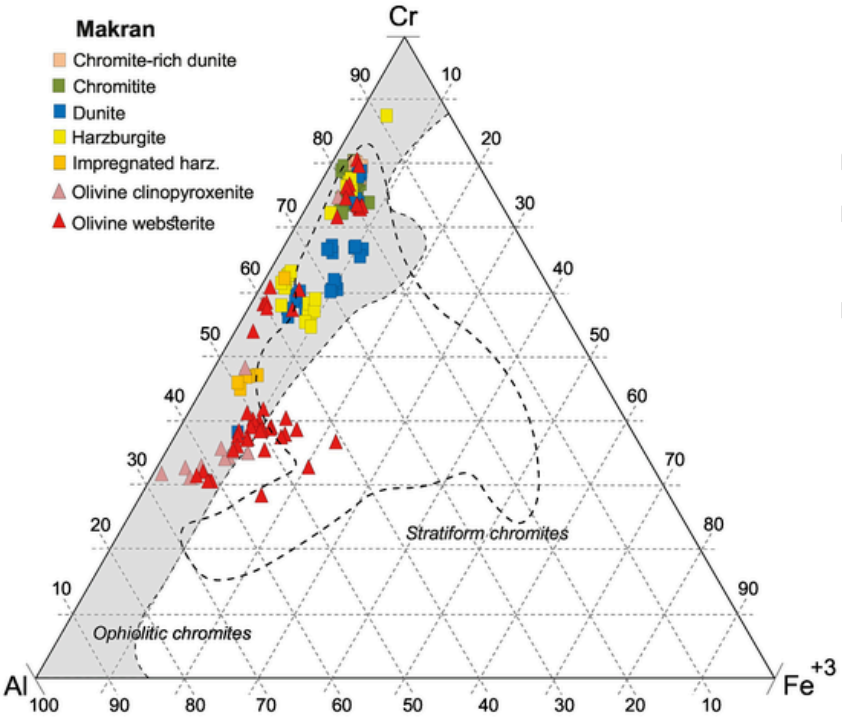

Fig. 7. Composition of chromites from different rocks units of the Sorkhband ultramafic complex in a Cr-Al-Fe^{3+} diagram. Fields of stratiform and ophiolitic chromitites are from Qasim Jan and Windley (1990).

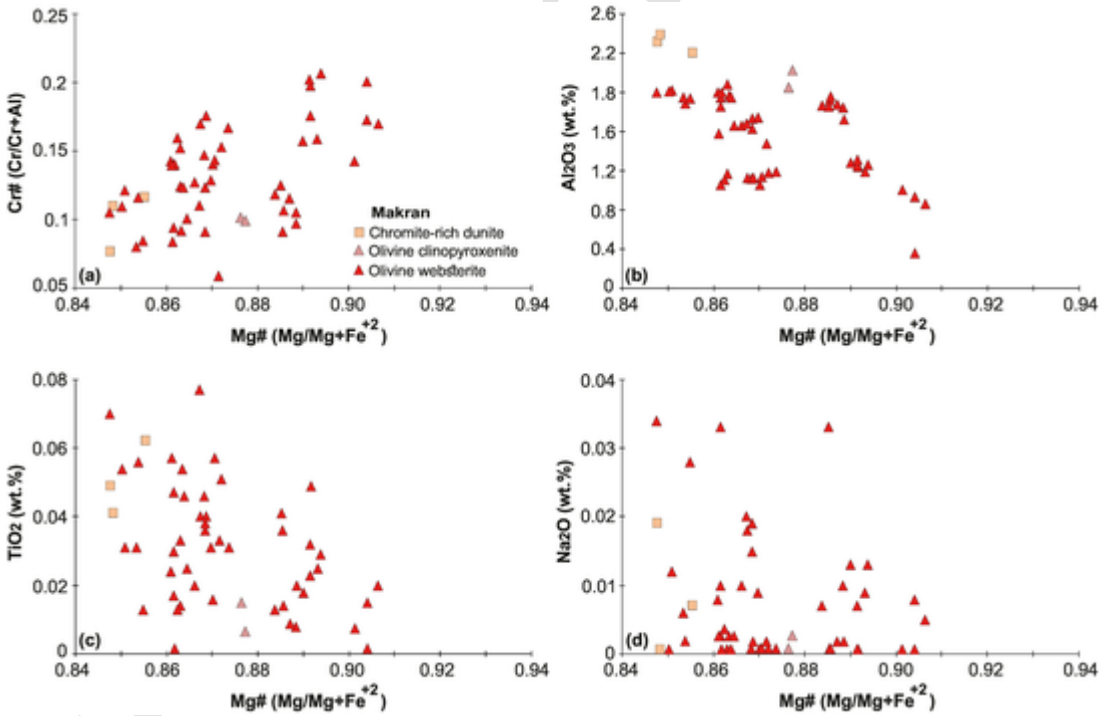

Fig. 8. Cr# (Cr/Cr + Al) (a), Al_2O_3 (b), TiO_2 (c) and Na_2O (d) vs Mg# (Mg/Mg + Fe^{+2}) compositional variations for orthopyroxene from different rocks units of the Sorkhband ultramafic complex.

with Mg# = 0.93–0.94, Cr# = 0.22–0.23, Al_2O_3 = 1.1 wt%, Na_2O = 0.22–0.25 wt% and TiO_2 = 0.03–0.06 wt% (Fig. 9). One clinopyroxene grain in chromite-rich dunite sample F13–33 has high Mg# (0.97), Cr# (0.39) with low contents of Al_2O_3 (0.56 wt%) but high Na_2O (0.29 wt%) and CaO (26.3 wt%) compared to other clinopyroxenes, which seem to have a metasomatic origin.

Clinopyroxenes in harzburgites have Mg# = 0.90–0.96, Cr# = 0.17–0.43, Al_2O_3 = 0.37–1.35 wt%, Na_2O = 0.09–0.19 wt%, and TiO_2 < 0.09 wt% (Fig. 9). Impregnated harzburgites have quite different clinopyroxenes, with lower Mg# (0.90–0.92) and Cr# (0.14–0.19), but higher Al_2O_3 (1.63–2.3 wt%), Na_2O (0.12–0.17 wt%), and TiO_2 (0.09–0.13 wt%). Clinopyroxenes in olivine clinopyroxenites have Mg# = 0.91–0.93, Cr# = 0.08–0.16, Al_2O_3 = 1.46–2.40 wt%,

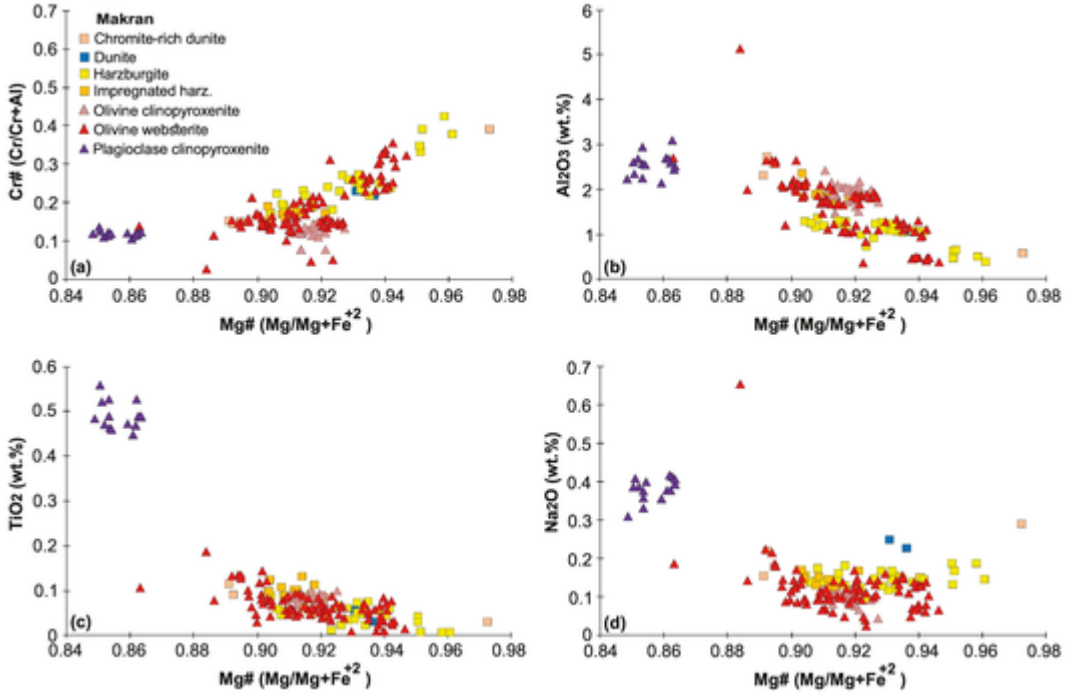

Fig. 9. Cr# (Cr/Cr + Al) (a), Al_2O_3 (b), TiO_2 (c) and Na_2O (d) versus Mg# (Mg/Mg + Fe^{+2}) compositional variations for clinopyroxene from different rocks units of the Sorkhband ultramafic complex.

Na_2O = 0.05–0.14 wt% and TiO_2 = 0.05–0.10 wt% (Fig. 9). In contrast, olivine websterites have clinopyroxenes with various compositions with Mg# = 0.86–0.95, Cr# = 0.03–0.36, Al_2O_3 = 0.36–5.1 wt%, Na_2O = 0.02–0.65 wt% and TiO_2 < 0.19 wt% (Fig. 9). Clinopyroxenes from plagioclase-bearing clinopyroxenites have low Mg# (0.85–0.86) and Cr# (0.11–0.14), but high Al_2O_3 (2.1–3.1 wt%), Na_2O (0.31–0.41 wt%) and TiO_2 (0.45–0.56 wt%) (Fig. 9).

5.2.5. Amphibole

Amphiboles in olivine websterites have Mg# ranging from 0.86 to 0.90. Although their textures show that these amphiboles are magmatic and have crystallized both before (as inclusions in clinopyroxene) and after clinopyroxene (interstitial between clinopyroxenes), it is important to know whether these amphiboles are compositionally similar to the magmatic amphiboles or are alteration products of the clinopyroxene. For this purpose, their mineral formulae were re-calculated following the nomenclature proposed by Hawthorne et al. (2012) and the spreadsheet supplied by Ridolfi et al. (2010). This calculation indicates that amphiboles from olivine websterites are high-Si, high-Al and/or high-Cr magnesio-hornblendes, with ~0.13–0.28 apfu Na cation (atoms per formula unit = apfu) in site A, but with 1.88–1.96 Ca and 0.04–0.11 Na cations in site B and 0.02–0.03 Ti in Site C and were in equilibrium with calc-alkaline melts.

The $Al^{(T)}$ (total Al = $^{[6]}Al + {}^{[4]}Al$) of these amphiboles ranges between 1 and 1.5, with Al# (= $^{[6]}Al/{}^{[T]}Al$) between 0.20 and 0.30. They have higher Al# values than amphiboles from shallow magmatic rocks and/or those produced by alteration of clinopyroxene (with Al# = 0). Their Al# values are comparable to those of high-P crustal and/or mantle-derived (experimental) amphiboles (with Al# = 0.21) (Ridolfi et al., 2010).

5.2.6. Garnet

Garnet in the Sorkhband complex occurs both as Cr-rich garnets (Cr_2O_3 = 17.4–18; uvarovite) in veins and/or interstitial to the chromite grains in stratiform chromitites and as hydrogrossular (Al_2O_3 = 25.1–30.8, CaO = 16.7–27.4), an alteration product of plagioclase in plagioclase-bearing clinopyroxenites.

5.2.7. Mineral inclusions

Mineral inclusions are rare in chromite grains of the Sorkhband chromitites. The most abundant inclusions are olivine and clinopyroxene. Olivine inclusions have forsterite contents of ~97.7 with NiO = 0.69–0.78 wt%.

5.2.8. Sulphides

Representative composition of sulfides (±oxides and alloys) is reported in Supplementary Table S3. The Sorkhband olivine websterites, olivine clinopyroxenites, plagioclase-bearing clinopyroxenites and stratiform chromitites contain Fe-Ni alloys (Supplementary Fig. S2c; or probably Fe-Ni carbides as found in the deep mantle of Tibetan ophiolites; e.g., Griffin et al., 2016), Fe-Co alloys (Supplementary Fig. S2f), pyrites or pyrrhotite (Supplementary Fig. S2c-e), pentlandites (Supplementary Fig. S2d) and monosulphide solid solutions, containing mostly Fe but with minor amounts of Ni, along with millerite, magnetite and ferritchromites (Supplementary Fig. S2e).

5.3. Trace elements in clinopyroxene

Chondrite-normalized rare earth element (REE-) patterns of clinopyroxenes from olivine clinopyroxenites and olivine websterites are quite different, but all are depleted in the light and middle REEs (LREE-MREE; Fig. 10). Enrichments in all trace elements, especially HREEs to MREEs, differ among the samples; some have higher contents of HREE- to MREE and concave-upward HREE-MREE patterns (with $Eu_{(n)}/Lu_{(n)}$ = 0.7–1.2) such as samples F13–31 and FB14–31, whereas some samples such as F13–8, FB14–7, FB14–10 and FB14–20 are quite depleted in all REEs and have flat patterns of the MREE (Gd) to HREE (Lu) ($Gd_{(n)}/Lu_{(n)}$ = 0.7–1.4), and more depleted patterns from La to Eu ($La_{(n)}/Eu_{(n)}$ = 0.03–0.2). These clinopyroxenes are enriched in MREEs to HREEs compared to clinopyroxenes from supra-subduction zone peridotites (Pearce et al., 2000b). The Sorkhband clinopyroxenes are depleted in Zr and Hf (Fig. 11), but enriched in Sr, Ti, Sc, V and Cr and

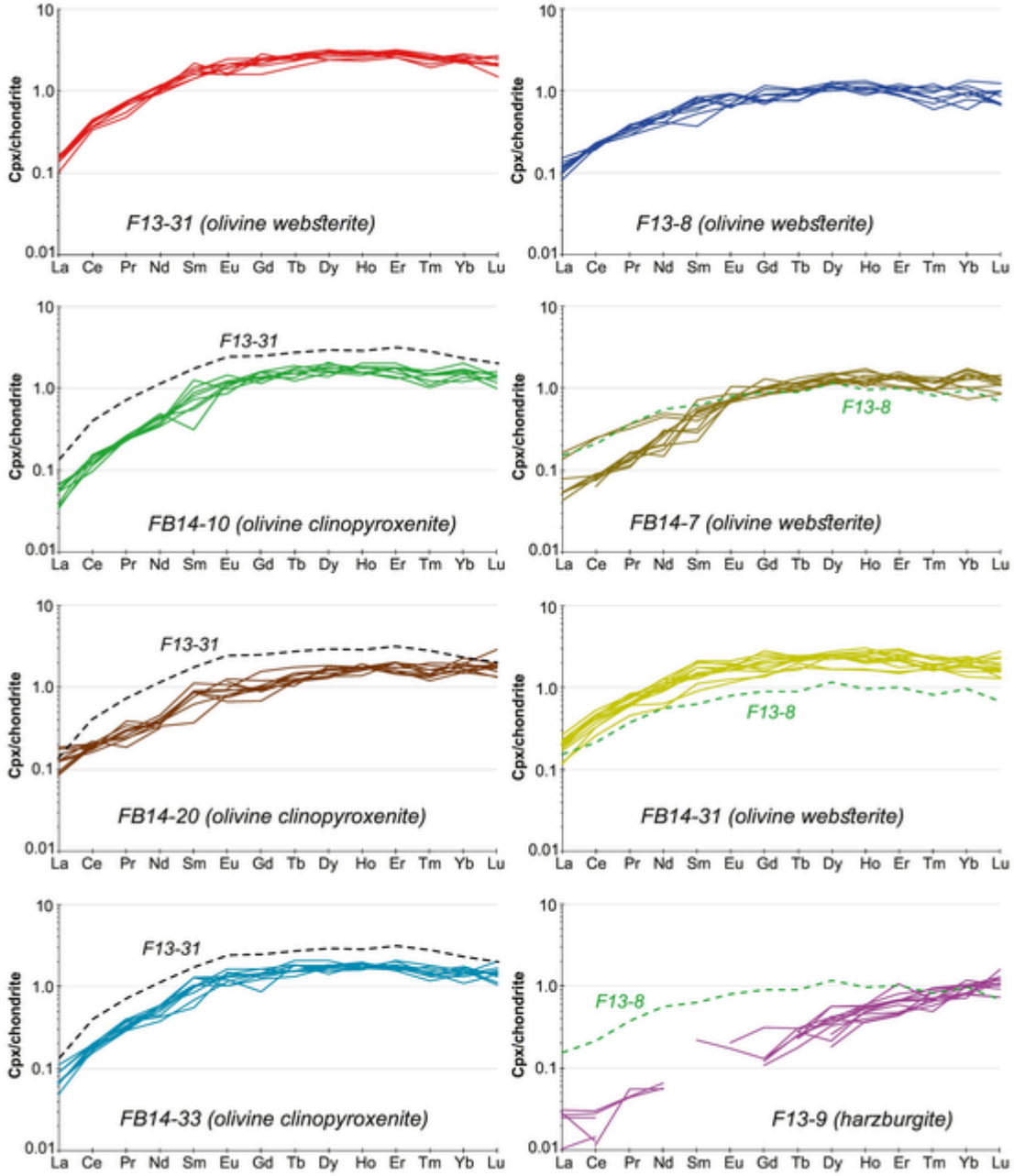

Fig. 10. Rare earth elements concentration in clinopyroxenes from harzburgites, olivine websterites and olivine clinopyroxenites of the Sorkhband ultramafic complex, analyzed by laser ablation ICP-MS.

some fluid-mobile elements such as B, Pb, Li and Rb. Enrichment in highly compatible elements such as Sc, Cr and V, relative to the HREE, indicates their compatibility and accumulation in clinopyroxene.

Clinopyroxene in Sorkhband harzburgite sample F13–9 exhibits REE patterns different from those of clinopyroxene in olivine clinopyroxenites and olivine websterites. Harzburgite clinopyroxenes show strong depletion in all REEs with a steep trend from Lu to Dy (and to La) (with $Dy_{(n)}/Lu_{(n)} = 0.2–0.5$). The trend is similar to the REE patterns of supra-subduction zone peridotite clinopyroxenes. Harzburgite clinopyroxenes have high contents of Cr, V and Sc but are highly depleted in other trace elements and fluid-mobile elements, mostly below the detection limit of these elements.

6. Discussion

6.1. Deformation styles

Our EBSD results are summarized here and in Table 1. Both dunites (samples F13–5 and FB14–19) present evidence for plastic deformation in their olivines (i.e., fabric, undulose extinction, subgrains and kinks). The combination of fabric and internal deformation features are all consistent with high-temperature deformation probably in the crust-mantle boundary conditions (Henry et al., 2017; Spiess et al., 2017). We observed a difference in the internal deformation recorded between two samples; sample FB14–19 displays more internal strain than sample FB13–5 which shows some degree of textural recovery.

Chromitite sample FB14–4 has a large modal fraction of chromite and shows a trace of internal strain within both olivine and chromite. The presence of a bimodal distribution of grain size and the difference

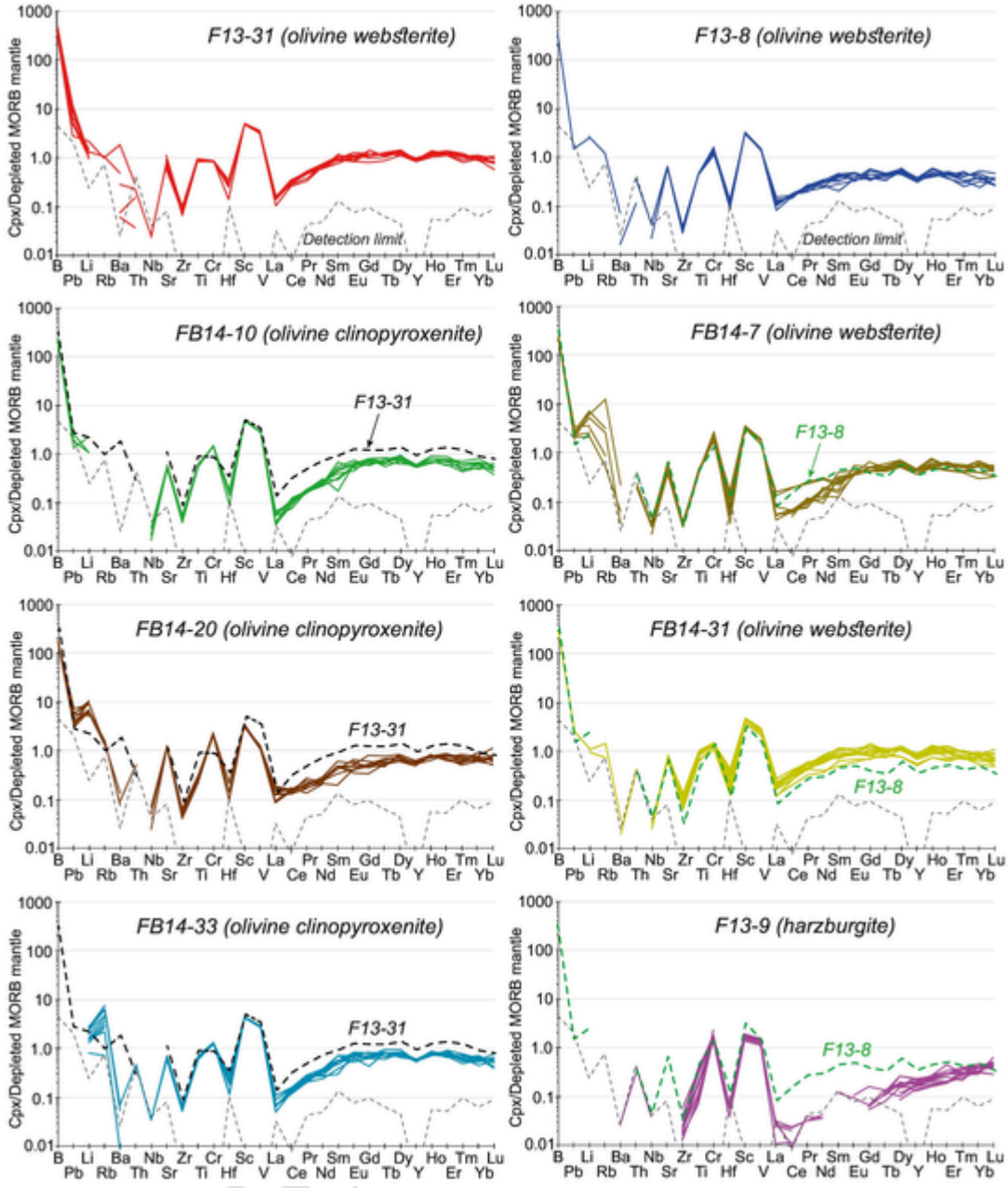

Fig. 11. Rare earth elements concentration in clinopyroxenes from harzburgites, olivine websterites and olivine clinopyroxenites of the Sorkhband ultramafic complex, analyzed by laser ablation ICP-MS. All data have normalized to depleted MORB mantle (Salters and Stracke, 2004).

in internal strain between two grain fractions of chromites suggest that both plastic deformation and recrystallisation occurred. It seems that chromitites were deformed in the same event recorded by dunites. Olivine in the chromitites recorded plastic deformation in the form of undulose extinction, subgrains and kink bands. The [010]-fabric of these olivines could be interpreted in different ways, e.g., either a magmatic or a plastic deformation origin for this fabric (Jung and Karato, 2001). Considering the important internal strain observed in every phase and the lack of a textural equilibrium we suggest that this fabric resulted from plastic deformation of olivine.

Olivine pyroxenites and websterites have less conspicuous internal deformation than other rocks and show the strongest level of textural equilibrium in our samples. However, the presence of non-random fabrics in clinopyroxene and orthopyroxene points could record a plastic deformation. In contrast, the textures of pyroxenites and websterites have extensively recovered, which probably indicates crystallization from a "melt mush" in the melt conduits/dikes.

6.2. Subsolidus exchange and/or changes in magma chemistry

The chemical compositions of minerals from different rock units of the Sorkhband complex show significant variations, both within individual samples and throughout the complex. Geochemical variations include changes in olivine Mg# and NiO content, spinel Cr#, Mg# and TiO_2 and clinopyroxene Cr#, Mg#, TiO_2 and Al_2O_3 ($\pm$ Na_2O) abundances across dunites, chromite-rich dunites, chromitites, olivine clinopyroxenites and webstrites. Further to these geochemical variations, plagioclase-bearing clinopyroxenites have completely different Cr#, Mg#, TiO_2, Al_2O_3 and Na_2O compared to other rock types. These geochemical variations are not systematic and do not seem to be related to the modal proportions of chromite, olivine (e.g., in dunites or

Table 1
Deformation style of the selected Sorkhband samples analyzed using EBSD.

Rock type	F13–5	FB14–19	FB14–4	F13–7	FB14–7	FB14–33
	Dunite	*Dunite*	*Chromitite*	*Olivine websterite*	*Olivine websterite*	*Olivine clinopyroxenite*
Internal deformation markers	Undulose extinction / Kink bands / Subgrains / Weak Shape Prefered Orientation	Undulose extinction / Subgrains / Kink bands / Shape Prefered Orientation	Subgrain boundaries in large chromite grains	Scarce subgrains	Undulose exctinction / Subgrains	Scarce subgrains
Grain size distribution	Unimodal	Bimodal	Bimodal	Unimodal	Bimodal	Bimodal
Textural recovery	Advanced	Limited	Limited	Advanced	Limited	Advanced
Olivine CPO	[100]-fibre	Non-random	[010]-fibre	–	Random	Non-random
Cpx CPO	–	–	–	Random	Random	Non-random
Opx CPO	–	–	–	Random	–	Non-random

chromitites, although some minerals of these rocks could show traces of subsolidus exchange) and clinopyroxene (e.g., in clinopyroxenites and websterites) in different rocks, but instead these show changes in the magma chemistry (e.g., in different samples of the same rock type) and/or changes in percolating melts (e.g., in impregnated samples or within samples that show two generations of a mineral with different chemistry).

These variations in the major elements of these minerals could also show re-equilibration between different phases to various extents. For example, the Mg# of clinopyroxene can be slightly increased due to re-equilibration with olivine in harzburgites and probably in olivine websterites (e.g., Belousov et al., 2021). The Mg-Fe^{+2} distribution between olivine and clinopyroxene is supposed to be variable and dependant on the equilibration temperature (Muroi and Arai, 2014). In the Sorkhband ultramafic complex, the Fe-Mg distribution diverges slightly from unity and thus the Fe# is slightly higher in olivine (olivine average Fe# = 12.7 in harzburgites and 13.3 in olivine websterites and clinopyroxenites) than in coexisting clinopyroxene (clinopyroxene average Fe# = 7.1 in harzburgites and 8.2 in olivine websterites and clinopyroxenites). This is indicative of subsolidus temperatures at *ca* 800 to 900 °C for the olivine-clinopyroxene pairs, which means that the initial Mg# has changed in both olivine and clinopyroxene during cooling to the subsolidus temperature. However, the olivine websterites do not have high modal contents of olivine that might promote re-equilibration and lead to such big geochemical variations in the clinopyroxene of olivine websterites.

Plagioclase-bearing clinopyroxenite sample FB14–28 has different clinopyroxene composition than other rocks, and this can be strongly influenced by the presence of plagioclase in these samples. However, the high Al_2O_3, TiO_2, Na_2O but low Cr# and Mg# of the clinopyroxene in sample FB14–28 cannot be explained by re-equilibration and/or by co-precipitation with plagioclase; instead, it shows crystallization from a different melt compared to clinopyroxene from other Sorkhband rocks. In addition, the clinopyroxene Al_2O_3 and TiO_2 contents can be changed by subsolidus exsolution of oxides (spinel group and/or Ti-rich oxides) from clinopyroxene. In the Sorkhband plagioclase-bearing clinopyroxenites, the absence of such exsolution rule out this idea. We also emphasize that the strong variations in Mg# of olivine and spinel from dunites and stratiform chromitites along the Sorkhband dunitic transition zone are not correlated with either presence or absence of impregnating clinopyroxene, and this suggests that re-equilibration with impregnating melts is not the cause of these variations. There is also no trace of gabbroic veins or strong impregnation in dunites and chromitites that could cause such variations. We therefore suggest that the compositional variations in olivine and spinel in dunites and stratiform chromitites are partly related to different magmatic pulses with distinctive geochemical signatures. However, we should emphasize that the Mg# of spinel could change via Mg-Fe distribution with olivine (e.g., Arai and Miura, 2016; Kapsiotis et al., 2018). The Mg# of spinel and olivine in chromitites and dunites tends to be higher than that in associated peridotites, depending on both the equilibrium temperature and the modal proportion (Arai, 1980).

Alteration of spinel grains could also affect their Mg#, but the alteration cannot be detected in the electron back-scattered images and our analyses are also far from the rims of spinels. The high forsterite contents (>94) of olivines in Sorkhband chromitites and chromite-rich dunites can reflect subsolidus cooling and low modal abundance of olivine compared to the high modal chromite, which could facilitate more subsolidus exchanges (Arai, 1980; Miura et al., 2012). Some of olivines with high forsterite also have NiO contents >0.5 wt%, which could again result from subsolidus redistribution with the surrounding spinel.

6.3. Formation mechanisms of olivine clinopyroxenites and websterites

6.3.1. Geochemical variations

Olivine websterites and olivine clinopyroxenites are common in supra-subduction zone-related ophiolites such as Oman (Tamura and Arai, 2006) and Voykar ophiolite of Polar Urals (Belousov et al., 2021) and fossilized subduction zones such as Cabo Ortegal (Tilhac et al., 2017) and Kuhistan (Garrido et al., 2007); they occur as dikes or small intrusive pockets within the mantle section and as cumulate-like bodies or dikes within the mantle-crust transition zone. These rocks (pyroxenites and websterites ± wehrlites) along with cumulate dunites are also interpreted as cumulates and/or reaction products between the melt and mantle harzburgite within the MOHO transition zone (e.g., Koga et al., 2001; Negishi et al., 2013).

The contacts of the Sorkhband olivine websterites and olivine clinopyroxenites with surrounding dunites and harzburgites (±chromitites) are sharp and these dikes appear to have been injected into the host peridotites during late magmatic phases and/or during the uplift of the Sorkhband ultramafic complex. The mineral compositions of these rocks can help to understand the formation mechanism of olivine websterites and olivine clinopyroxenites. For example, the contents of HREE in clinopyroxene could reflect the compositions of parental melts, source fertility and/or extent of melting/fractionation. Clinopyroxene from most Sorkhband olivine websterites and olivine clinopyroxenites displays enrichment in HREE (as well as in Ti, Al_2O_3 and $Ce_{(n)}/Yb_{(n)}$) but overall, they have lower HREE than abyssal peridotites and/or MORBs. There are also pronounced positive anomalies of V, Sc, Ti, Cr, Sr and Pb in clinopyroxenes (Fig. 11).

The low Al_2O_3 contents and low but variable Na_2O and TiO_2 of clinopyroxenes from the Sorkhband complex (except the plagioclase-bearing clinopyroxenite sample FB14–28) suggest formation in a supra-subduction zone setting, but from >1 magmatic pulse. Clinopyroxenes from plagioclase-bearing clinopyroxenites with low Mg# (0.85–0.86) and Cr# (0.11–0.14), but high Al_2O_3 (2.1–3.1 wt%), Na_2O (0.31–0.41 wt%) and TiO_2 (0.45–0.56 wt%) differ in composition from other clinopyroxenes and appear to have crystallized from a different melt. The variations in the Na_2O, TiO_2 and Al_2O_3 abundances could be

related to changes in the H_2O contents of host magmas in a supra-subduction zone setting. The presence of amphibole suggests that supra-subduction zone-related fluid-rich melts were involved during the formation of Sorkhband olivine websterites and olivine clinopyroxenites. However, Tamura et al. (2014) found amphibole-dominant inclusions in chromite from metasomatized harzburgites and the troctolites formed by harzburgite-magma reaction in the Mid-Atlantic Ridge. These indicate that the peridotite-magma interaction can also concentrate H_2O, Na and other incompatible elements even in the MORB-peridotite system, which is poor in H_2O (Arai et al., 1997).

To further check the nature of magmas which produced olivine websterites and olivine clinopyroxenites, we have used plots of Ti, Al_2O_3 and $Ce_{(n)}/Yb_{(n)}$ vs $Yb_{(n)}$. These plots show that the clinopyroxenes from Sorkhband rocks are similar to clinopyroxenes from the low-TiO_2 fore-arc basalts of the Hunter subduction system, but most of them resemble those in boninites from Troodos, Hunter and Tonga fore-arc systems (Fig. 12). The similarities between the clinopyroxenes of Sorkhband olivine websterites and olivine clinopyroxenites and those of the Troodos and/or Hunter and Tonga fore-arc basalts and boninites could indicate that the Sorkhband olivine websteritic and olivine clinopyroxenitic dikes formed in a supra-subduction zone setting. In addition, the clinopyroxenes crystallized from supra-subduction zone-related and/or boninitic melts are depleted in total HREE including Dy and Yb (Jean et al., 2010). Clinopyroxenes from Sorkhband olivine websterites and clinopyroxenites also have very low Dy (<0.8 to <0.5 ppm) and Yb (<0.5) contents, consistent with melts from a depleted fore-arc mantle (Fig. 13).

Spinel from Sorkhband olivine websterites and olivine clinopyroxenites could also be used as a petrogenetic index (Arai, 1994; Kamenetsky et al., 2001; Saccani and Tassinari, 2015). Spinel in Sorkhband olivine websterites and olivine clinopyroxenites has compositions ranging from low to high Cr# and Mg#. Spinel Cr# is strongly dependent on the alumina content of the host magmas as well as the crystallization pressure (Belousov et al., 2021). Since all ultramafic dikes occur nearly in the same mantle-crust boundary level in the Sorkhband complex, we suggest that the spinel geochemical variations could reflect crystallization from the supra-subduction zone-related melts, but with variable compositions. The chemical composition of spinel has been used by many authors to constrain the composition(s) of their parental melts. We therefore used the formulae proposed by Rollinson (2008) for calculating the TiO_2 and Al_2O_3 contents in the parental melts from which spinels crystallized (see Supplementary Table S1). The parental liquid composition calculated using spinels in olivine clinopyroxenites have variable TiO_2 contents (0.21–0.61 *wt*%) and high Al_2O_3 contents (16.60–18.06 *wt*%). These values overlap the compositional variation of boninitic and IAT (or FAB-like) melts (Saccani et al., 2018b; Saccani and Tassinari, 2015). Likewise, the calculated TiO_2 and Al_2O_3 contents for olivine websterites show that these rocks may have derived from different melt compositions. A couple of olivine websterites (F-13-8 and FB-14-7) display calculated TiO_2 (0.21–0.34 wt%) and Al_2O_3 (10.79–14.41 wt%) contents, which are similar to those of boninitic basalts (TiO_2 = 0.1–0.5 wt%. Al_2O_3 = 8–14 wt%; Saccani et al., 2018b; Saccani and Tassinari, 2015). In contrast, most olivine websterites display calculated TiO_2 (0.42–0.89 wt%) and Al_2O_3 (14.71–17.68 wt%) contents, which are similar to those of IAT/FAB melts (TiO_2 = 0.5–0.8 wt%; Al_2O_3 = 14–16 wt%). Evidence from spinel TiO_2 and Al_2O_3 compositions further support the hypothesis that olivine websterites and clinopyroxenites may have crystallized in a supra-subduction zone setting from compositionally different melts.

6.3.2. Formation mechanisms

Olivine websterites and clinopyroxenites could form in several ways: crystallization of mantle-derived melts formed within the surrounding peridotites (Tamura and Arai, 2006); crystallization and crystal accumulation occurred within melt conduits, from migrating melts formed in different parts of the mantle (Downes, 2007) and accumulation from primitive arc magmas, near the crust-mantle boundary (Berly et al., 2006). Crystallization of mantle-derived boninitic melts formed within surrounding peridotites has been proposed based on similarities in mineral chemistry between pyroxenites and mantle harzburgites in Oman ophiolites (Tamura and Arai, 2006). This mechanism is unlikely for the Sorkhband case since most minerals from these rocks have different mineral major- and trace-element chemistry than those in the host harzburgites. Crystallization of hydrous basaltic andesites and high-Mg# andesites at 1.2 GPa and 1030 to 1230 °C could produce pyroxenites to websterites (Downes, 2007). The presence of H_2O and high-pressure conditions suppress plagioclase crystallization and

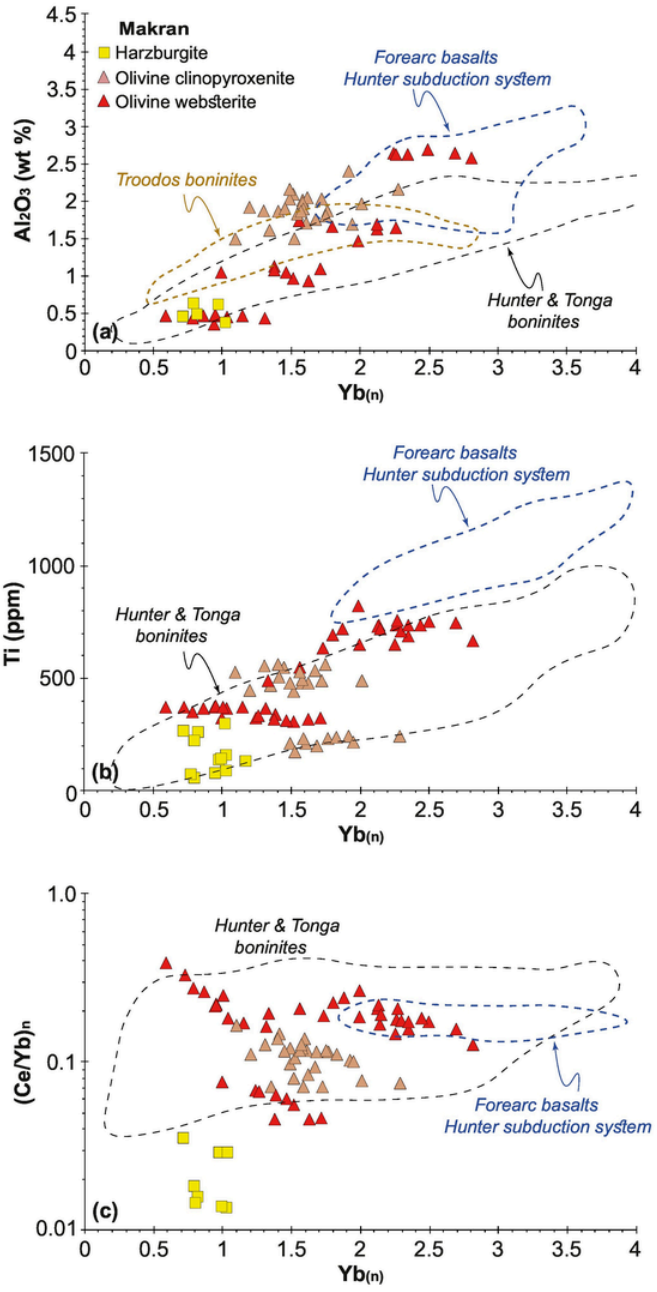

Fig. 12. Al_2O_3 (wt%), Ti (ppm) and $Ce_{(n)}/Yb_{(n)}$ ratio vs $Yb_{(n)}$ (n = normalized to chondrite) for clinopyroxenes from Sorkhband harzburgites, olivine websterites and olivine clinopyroxenites. Fields for low-Ti forearc basalts and boninites from the Hunter subduction system and Hunter, Tonga and Troodos boninites are from Belousov et al. (2021).

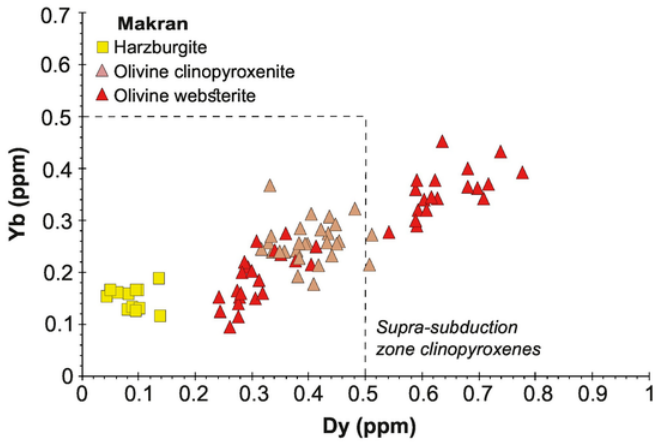

Fig. 13. Yb and Dy concentrations in clinopyroxenes from Sorkhband harzburgites, olivine websterites and olivine clinopyroxenites. The field for supra-subduction zone peridotites is from Jean et al. (2010).

favours pyroxene crystallization. Some olivine clinopyroxenites and websterites show cumulate-like textures, suggesting crystal accumulation may have occurred within dikes/melt conduits.

Different Mg# of minerals in different olivine clinopyroxenites and websterites could reflect wall-rock reaction at different melt/rock ratios. However, the sharp contacts of late-stage clinopyroxenite and websterite dikes with peridotite wall-rocks and the lack of reaction textures, are not consistent with formation of clinopyroxenites and websterites by extensive melt-rock reaction at their site of emplacement. We believe that variations in mineral chemistry of the Sorkhband olivine clinopyroxenites and websterites, along with variable HREE in clinopyroxene, are more consistent with significant changes in their parental melts. Such changes could reflect the evolution of melts through melt-peridotite reactions at deeper levels and/or could represent different melt pulses coming from an evolving subduction zone. Magmatic fractionation within the mantle can reconcile the variations in TiO_2, Na_2O and Al_2O_3 abundances versus Mg# and/or Cr# of clinopyroxene and orthopyroxene of same rocks (e.g., in olivine websterites, Figs. 8–9) but this mechanism cannot explain the different REE patterns (especially HREE to MREE trends) of clinopyroxenes or the variations in spinel Cr# at a given Mg# (Fig. 14a).

6.4. Sorkhband harzburgites

The supra-subduction zone peridotites are characterized by spinels with higher Cr# than abyssal peridotites, which indicates higher degrees of partial melting in the mantle-wedge peridotites (Arai, 1994; Gaetani and Grove, 1998). The content of TiO_2 in spinel is also a good indicator of the tectonic setting from which chromite-bearing magmas have issued, e.g., arc vs mid-ocean ridge (Arai et al., 2011). Clinopyroxenes in the supra-subduction zone or fore-arc peridotites are characterized by low Al_2O_3, Na_2O, TiO_2 and HREEs but high Cr# and Mg# compared to clinopyroxene in abyssal peridotites (Pearce et al., 2000b). Some harzburgite spinels have high Cr# and plot in the field of fore-arc peridotites (Fig. 14a) and their clinopyroxenes have high Mg# and Cr# but low Al_2O_3, Na_2O, TiO_2, along with a steep depleted pattern from Lu to Gd (Figs. 10-11), which also indicates a high degree of partial melting of peridotites. These geochemical variations in clinopyroxene compositions (along with their irregular and resorbed shape) show that these types of clinopyroxene are residual. The Yb and Dy contents of the analyzed harzburgite clinopyroxenes are very low (Fig. 13), consistent with melting residues. There is a clear correlation between spinel Cr# and clinopyroxene Cr# in the harzburgites (Fig. 15a). However, some spinels from harzburgites and impregnated harzburgites plot outside the mantle-peridotite field and follow a fractionation trend in the plot of spinel Cr# vs olivine Mg#. These signatures along with low Mg# and Cr# but high Al_2O_3, Na_2O, TiO_2 probably reflect crystallization from percolating melts, with compositions different from MORBs.

Plots of spinel Cr# vs TiO_2 (Fig. 15b) show that the Sorkhband impregnated harzburgites, as well as some harzburgites (except those with residual clinopyroxene), dunites and stratiform chromitites reacted more extensively with percolating melts during porous flow and crystalized high- TiO_2 spinels. These plots suggest that the percolating melts changed with time from boninites to arc tholeiites.

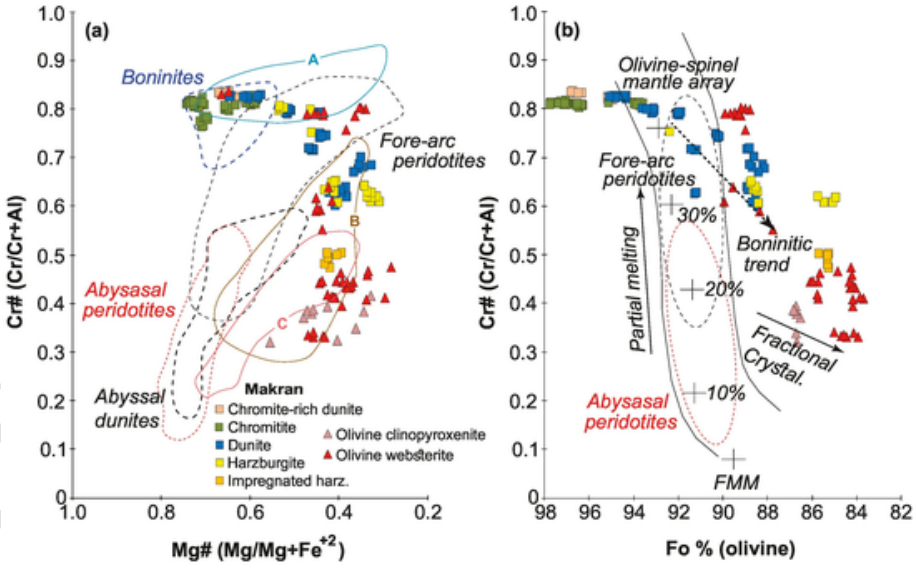

Fig. 14. Plot of spinel Cr# vs spinel Mg# (a) and spinel Cr# vs olivine forsterite (b) in Sorkhband ultramafic rocks. Olivine-spinel mantle array and melting trends (in %) are from Arai (1994). Fields for boninites, forearc and abyssal peridotites are from Dick and Bullen (1984); Parkinson and Pearce (1998b); Pearce et al. (2000a). Fields A, B and C are from Saccani and Tassinari (2015). A = Boninite-influenced compositions; B = Medium-Ti basalts and island arc tholeiite-influenced compositions; C = MORB and medium-Ti basalt influenced composition. Medium-Ti basalts are similar to the fore-arc basalts of Reagan et al. (2010), from Izu-Bonin-Mariana subduction system.

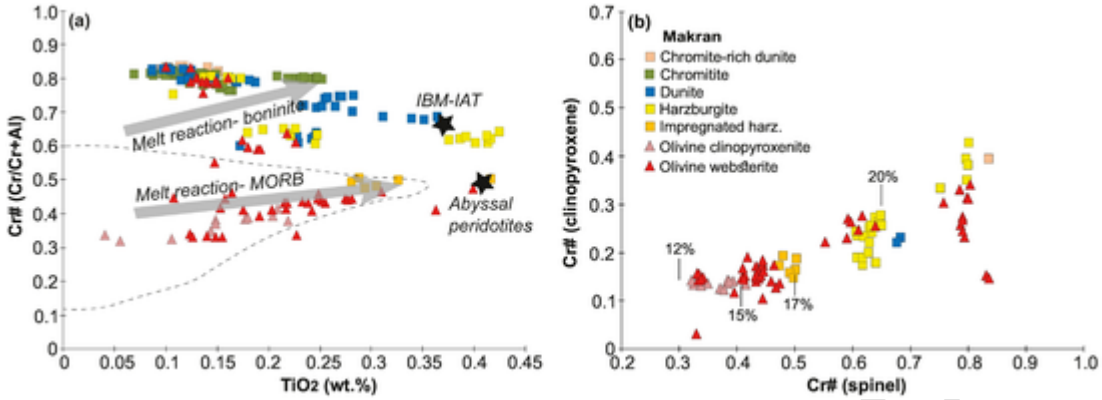

Fig. 15. Spinel Cr# vs TiO_2 (a) and spinel Cr# vs clinopyroxene Cr# (b) for Sorkhband ultramafic rocks. The thick grey arrows show the effect of melts (with the composition of Troodos boninites and abyssal basalts) on refractory subduction-zone peridotites. Compositions of Izu-Bonin-Mariana island arc tholeiites and abyssal peridotites are from Pearce et al. (2000b). Equivalent melt fractions correlated with spinel Cr# in panel (B) are calculated according to Hellebrand et al. (2001).

6.5. Origin of the various types of dunites

The ophiolitic dunitic transition zone in ophiolites is usually considered to mark the crust-mantle boundary and is a dunite-dominated zone with some mafic intervals including gabbroic and pyroxenitic dikes and magmatic impregnations (Abily and Ceuleneer, 2013; Arai and Matsukage, 1996; Dick and Natland, 1996). The Sorkhband complex differs in some ways from this definition, but the presence of stratiform chromitites, dunites, olivine clinopyroxenites and websterites and their stratigraphic position below the layered gabbros suggest that the complex is a mantle-crust dunitic transition zone. The presence of *syn*-magmatic folding and faulting in stratiform chromitites, lack of strong solid-state deformation, their layered structure and local gradational layering of chromite-rich layers suggest crystallization of an ultramafic-basic melt in the mantle-crust transition zone to make a pile of layered cumulates which grade upward into the overlying gabbroic cumulates.

The most commonly proposed origins of the dunitic rocks in the transition zone include: (1) reaction of orthopyroxene-undersaturated MORBs, or SSZ-like melts migrating through peridotites (e.g., Akizawa and Arai, 2014; Koga et al., 2001); (2) piles of ultramafic cumulates, resulting from fractional crystallization of picritic melts at the base of the oceanic crust (e.g., Elthon, 1979); (3) residues after high-degree partial melting of peridotites (Arai, 1994; Tamura and Arai, 2006). A residual dunite (model#3) would have required >40% partial melting, which is unlikely in the modern upper-mantle thermal regime. Mechanisms (1) and (2) are suggested to be responsible for the formation of dunites in the Oman ophiolite (Abily and Ceuleneer, 2013) as well as in the Albanian ophiolites (Saccani et al., 2018b; Saccani and Tassinari, 2015).

Dunites in the dunitic transition zone have a broader range in olivine composition than the mantle tectonites, e.g., the Sorkhband dunites have forsterite content of 88.1 to 93.6. and NiO = 0.13 to 0.41 wt%, comparable with dunites from the Oman dunitic transition zone (Fo ~87 to 91; Abily and Ceuleneer, 2013). Forsterite levels of 94.3 to 95.1 are also common in the Sorkhband dunites, mainly in dunites with higher modal content of spinel and/or in olivine grains close to large spinel crystals. Spinel Cr# is also variable in dunites from the Sorkhband complex (Cr# = 0.60 to 0.83), higher than in the Oman dunitic transition zone (~0.5; Abily and Ceuleneer, 2013), but comparable with Cr# values of spinels in the transition-zone dunites from the supra-subduction Albanian ophiolites (Cr# = 0.70–0.90; Saccani et al., 2018b; Saccani and Tassinari, 2015). Accordingly, the calculated TiO_2 (0.17–0.25 wt%) and Al_2O_3 (10.06–10.26 wt%) contents in the parental melt in equilibrium with these spinels are in the typical range of composition for boninitic basalts (Saccani et al., 2018b; Saccani and Tassinari, 2015).

All these observations allow us to suggest that a huge SSZ-related (boninitic) melt batch reached the base of the crust and crystallized cumulate dunites with low-Fo, low-NiO olivine and high-Ti, low-Cr# spinels. This mechanism is also proposed for the formation of some dunites from the Oman dunitic transition zone (Abily and Ceuleneer, 2013). However, before the formation of cumulate dunites, the SSZ-related melt infiltration and build-up within the lower oceanic crust/uppermost mantle (peridotite-melt interaction) could have dissolved peridotite orthopyroxene to accumulate high-Fo, high-NiO olivines. This mechanism could also explain the screens of depleted harzburgites with interaction dunites in the Sorkhband complex. Incongruent melting of orthopyroxene could weakly affect the Cr/Al and TiO_2 contents of the resulting melts and thus the composition of the crystallizing spinels.

6.6. Stratiform chromitites

6.6.1. Geochemical evaluation

Olivine in the stratiform chromitites show variable forsterite (93.6–97.7) and NiO (0.36–0.96 wt%) contents, comparable with olivine in the surrounding chromite-rich dunites (forsterite = 94.9–97.3, NiO = 0.32–0.71 wt%) but higher than the forsterite and NiO content of olivine in dunites (forsterite = 88.1–95.1, NiO = 0.13–0.50 wt%) and harzburgites (fosterite = 84.9–92.4, NiO = 0.15–0.26 wt%). As discussed in section 6–2, the $Mg\text{-}Fe^{+2}$ subsolidus exchange between chromite and olivine may be responsible for high the forsterite content of olivine in chromitites and chromite-rich dunites.

The Cr# values of chromite grains in the Sorkhband stratiform chromitites are high (0.76–0.83) but with variable TiO_2 (0.07 to 0.25 wt%) and are similar to those of the disseminated chromites in the surrounding dunites (Cr# = 0.60 to 0.83 and TiO_2 = 0.09 to 0.37 wt%) and chromite-rich dunites (Cr# = 0.82–0.84, TiO_2 = 0.09–0.15 wt%). These values are higher than in chromites from the stratiform chromites of Oman (Cr# = 0.49–0.60), but are similar to the podiform ore bodies and their host dunites from Oman ophiolites (Rollinson and Adetunji, 2015). The high TiO_2 contents of the chromites in the Oman stratiform chromitites (TiO_2 = 0.25–0.54 wt%) suggest the involvement of a MORB-like melt in the formation of the Oman stratiform chromitites (Borisova et al., 2012; Rospabé et al., 2019; Zagrtdenov et al., 2018), whereas the lower TiO_2 (0.07 to 0.25 wt%) of chromites in Sorkhband stratiform chromitites is more consistent with crystallization from supra-subduction zone melts. Furthermore, the TiO_2 and Al_2O_3 contents in the parental melts equilibrated with the stratiform chromitites range from 0.13 to 0.37 wt% and

from 10.24 to 11.82 wt%, respectively, thus suggesting a clear boninitic nature of the parental melts.

6.6.2. Formation of stratiform chromitites

Hypotheses for the formation of chromitite ore deposits in ophiolites include: (1) crystallization from chromium-oversaturated mafic melts in magma chambers at the base of oceanic crust and/or within the mantle; (2) mingling and/or mixing between chromium-saturated basaltic melts and acidic, silica-rich melts, probably through assimilation of crustal rocks by basaltic melts; (3) addition of volatiles including water-rich fluids into chromium-saturated basaltic melts (e.g., Arai and Yurimoto, 1994; González-Jiménez et al., 2014; Latypov et al., 2018). However, both processes 1 and 2 are not independent and process 2 can produce the melt of case 1. Chromite grains in some deposits contain hydrous, Na- (or Na and K-) rich silicate inclusions such as amphibole and mica, which can attest to the participation of volatiles and alkali-rich fluids and/or melts during chromite formation, or even chromitite formation by hydrothermal processes (e.g., Arai and Akizawa, 2014; Johan et al., 2017). Hydrous, arc magma-like magmas are supposed to be involved in the formation of chromitites based on hydrous mineral inclusions in the chromite grains (e.g., Khedr and Arai, 2016). This does not hold, however, because hydrous mineral inclusions in chromite also can be formed within the MORB-peridotite system (Arai, 1998). Stratiform chromitites from the Oman ophiolites were suggested to have formed via hybridization between the ascending MORB-like melts and fluids (Rospabé et al., 2019). The fluid phases were supposed to be seawater, heated through its downward infiltration into lower crustal sequences and contributing to hydrous melting of the country rocks to yield a trondhjemitic melt (Koepke et al., 2014; Rospabé et al., 2019).

The chromite grains from Sorkhband chromitites and dunites mostly contain anhydrous mineral inclusions and amphibole is rare as inclusion, suggesting that hydrous melts were not strongly involved in the formation of Sorkhband chromitites and dunites. However, some olivine pyroxenites and websterites contain amphibole crystals, which indicate that hydrous melts probably become more predominant later in the magmatic evolution of the Sorkhband complex. We favour a model that assumes the formation of the Sorkhband stratiform chromitites through the crystallization from chromium-oversaturated mafic, SSZ-related melts within the mantle-crust boundary zone. This melt can be responsible for dissolving peridotite orthopyroxene to generate dunites with high-forsterite, high-NiO olivines and high-Cr# spinels.

6.7. Melt evolution in the Makran subduction zone

The tectonic setting of the Makran ophiolites has remained controversial, but geochemical and geochronological evidence from magmatic rocks in the crustal section of these ophiolites shows that the Makran ophiolites contain both a Jurassic component including pillow lavas and gabbros with *E*-MORB and OIB geochemical signatures and a Late Cretaceous component with supra-subduction zone-related lavas, sedimentary and plutonic rocks (e.g., Barbero et al., 2020). The Late Cretaceous units are related to formation in a nascent arc, where Neotethyan subduction initiated beneath the Lut block during the Late Cretaceous; this was associated with rapid extension of the upper plate. The subduction initiation could build forearc oceanic crust with the eruption of forearc basalts, boninites and arc tholeiites (Reagan et al., 2017; Stern and Gerya, 2017).

This study shows that during the subduction initiation, the composition of the mantle melts that generate lithologies such as olivine websterites, olivine clinopyroxenites, dunites and stratiform chromitites, could be different even within a small region of the fore-arc mantle and this criterion should be related to both temporal changes in melt composition during subduction initiation and/or the processes taking place in the forearc mantle. Our geochemical data reveal that both mechanisms occurred simultaneously to produce variations in the Sorkhband ultramafic rocks and chromitites. However, the composition of spinels from some dunites, harzburgites, impregnated harzburgites, olivine clinopyroxenites and olivine websterites fall outside the fore-arc peridotite (Fig. 14a) and olivine-spinel mantle array fields (Fig. 14b), suggesting that crystal fractionations has affected boninitic or high-Mg# magmas to yield such variations in spinels and other major minerals. The HREE composition of the clinopyroxenes from Sorkhband olivine websterites and clinopyroxenites are also similar to those of boninitic melts, which could be derived from partial melting of hydrated peridotites in the mantle wedge of the fore-arc.

The last episode of magmatic activity in the Sorkhband complex produced plagioclase-bearing clinopyroxenites in which clinopyroxene has high TiO_2, Na_2O and Al_2O_3 but low Mg# and Cr#, and probably crystallized from a more enriched magma, compared to clinopyroxene from other olivine websterites and clinopyroxenites. This can show a change in magma chemistry during subduction initiation from early boninitic melts to arc tholeiites. These temporal magmatic variations from boninite to arc tholeiites are common in some fore-arcs such as the Tonga subduction system (Falloon et al., 2014) and/or in Troodos ophiolites (Cameron, 1985).

The absence of boninitic volcanic rocks in Sorkhband (and/or Makran) is an interesting point. However, we should emphasize that the north Makran is an accretionary belt, where ophiolites are not abducted, but are accreted into an accretionary prism. The rocks forming the different units of the north Makran were totally derived from the lower (i.e., subducting) oceanic plate and associated seamounts. These rocks also underwent subduction to various depths (from low pressure to the blueschist and eclogite facies). They were brought below the supra-subduction mantle wedge and then re-exhumed along the subduction channel. Therefore, the lack of boninites is probably due to the presence of the accretionary prism, which formed through the accretion of lower-plate rocks at shallow levels and/or lower-plate rocks exhumed along the Benioff zone. In this mechanism, HP-LT meta-oceanic basalts and the SSZ-mantle harzburgites (with chromitites) can be exhumed and accreted, whereas the upper-SSZ crust cannot be incorporated in this wedge.

7. Conclusions

The Makran accretionary complex in south Iran-Pakistan includes Jurassic and Late Cretaceous fossilized oceanic tracts. The Jurassic rocks have OIB-MORB geochemical composition, but Late Cretaceous rocks have supra-subduction zone-related geochemical characteristics and can be related to the initiation of the subduction of Neotethyan oceanic lithosphere beneath the Lut block during the Late Cretaceous. The mantle-crust transition zone in the Sorkhband ultramafic complex in western Makran contains depleted harzburgites, dunites, chromite-rich dunite and stratiform chromitites. All these units are injected by a series of crosscutting dikes, mostly of olivine websterite and olivine clinopyroxenite, but rarely with plagioclase-bearing clinopyroxenite. Major phases from these rocks include olivines, spinels, clinopyroxenes and orthopyroxenes with a wide range of compositions related to distinct processes operating in the mantle-crust transition zone of a nascent arc and related to the different magmatic pulses with different geochemical signatures. We have subdivided the main processes within the Sorkhband ultramafic complex into six main stages. First, during subduction initiation, the mantle rocks started to melt to produce supra-subduction zone-type magmas, leaving a depleted harzburgitic residue. Second, the melt infiltration and accumulation through the upper mantle and mantle-crust transition zone dissolved peridotite orthopyroxenes to make reaction dunites with high-forsterite, high-NiO olivines. Third, boninitic melts started to precipitate the cumulate dunites in the mantle-crust transition zone, which have low-forsterite, low-NiO olivines but high-Ti, low-Cr# spinels. Fourth, crystallization of chromium-oversaturated mafic melts within the mantle-crust boundary

produced stratiform chromitites. Fifth, several late-stage melt pulses with higher water content and with different compositions triggered the intrusion of dikes of olivine websterite, olivine clinopyroxenite and plagioclase-bearing clinopyroxenite. Sixth, infiltration of minor melt batches with different geochemical composition than other presumed melts were responsible for the formation of impregnation screens in harzburgites. All these geochemical variations in lithological units/geochemical signatures reflect the complex evolution of a forearc mantle during subduction initiation.

Supplementary data to this article can be found online at https://doi.org/10.1016/j.lithos.2021.106591.

Uncited reference

Sobolev and Danyushevsky, 1994

Declaration of Competing Interest

We have no pecuniary or other personal interest, direct or indirect, in any matter that raises or may raise a conflict of interest.

Acknowledgments

This study used instrumentation funded by ARC LIEF and DEST Systemic Infrastructure Grants, Macquarie University, NCRIS AuScope and Industry. This is contribution 1691 from the ARC Centre of Excellence for Core to Crust Fluid Systems (http://www.ccfs.mq.edu.au) and 1490 in the GEMOC Key Centre (http://www.gemoc.mq.edu.au). Financial support was also received from the Alexander von Humboldt Foundation in the form of a senior research grant and GEOMAR Helmholtz Centre to the first author while preparing these results for publication. We are very grateful to Ibrahim Uysal and Iain Neill for their constructive reviews of the manuscript. Editorial suggestions by Xian-Hua Li are also appreciated. All logistical supports for the fieldwork came from Damghan University, Iran. First author acknowledges the administration of the Faryab Mine for their hospitality and support. Also, first author would like to thank Mr. Shoghmand and Dr. Jamshidi for their help during the field work.

References

Abily, B., Ceuleneer, G., 2013. The dunitic mantle-crust transition zone in the Oman ophiolite: Residue of melt-rock interaction, cumulates from high-MgO melts, or both? Geology 41, 67–70.

Akizawa, N., Arai, S., 2014. Petrology of mantle diopsidite from Wadi Fizh, northern Oman ophiolite: Cr and REE mobility by hydrothermal solution. Island Arc 23, 312–323.

Arai, S., 1980. Dunite-harzburgite-chromitite complexes as refractory residue in the Sangun-Yamaguchi zone, western Japan. J. Petrol. 21, 141–165.

Arai, S., 1994. Characterization of spinel peridotites by olivine spinel compositional relationships - review and interpretation. Chem. Geol. 113, 191–204.

Arai, S., 1998. Comments of the paper "Primitive basaltic melts included in podiform chromites from the Oman ophiolite" by P. Schiano et al. Earth Planet. Sci. Lett. 156, 117–119.

Arai, S., Akizawa, N., 2014. Precipitation and dissolution of chromite by hydrothermal solutions in the Oman ophiolite: New behavior of Cr and chromite. Am. Mineral. 99, 28–34.

Arai, S., Matsukage, K., 1996. Petrology of gabbro-troctolite-peridotite complex from Hess deep, equatorial Pacific: Implications for mantle-melt interaction within the oceanic lithosphere. In: Proceedings-Ocean Drilling Program Scientific Results. National Science Foundation, pp. 135–156.

Arai, S., Miura, M., 2016. Formation and modification of chromitites in the mantle. Lithos 264, 277–295.

Arai, S., Yurimoto, H., 1994. Podiform chromitites of the Tari-Misaka ultramafic complex, southwestern Japan, as mantle-melt interaction products. Econ. Geol. 89, 1279–1288.

Arai, S., Matsukage, K., Isobe, E., Vysotskiy, S., 1997. Concentration of incompatible elements in oceanic mantle: effect of melt/wall interaction in stagnant or failed melt conduits within peridotite. Geochim. Cosmochim. Acta 61, 671–675.

Arai, S., Kadoshima, K., Morishita, T., 2006. Widespread arc-related melting in the mantle section of the northern Oman ophiolite as inferred from detrital chromian spinels. J. Geol. Soc. 163, 869–879.

Arai, S., Okamura, H., Kadoshima, K., Tanaka, C., Suzuki, K., Ishimaru, S., 2011. Chemical characteristics of chromian spinel in plutonic rocks: Implications for deep magma processes and discrimination of tectonic setting. Island Arc 20, 125–137.

Barbero, E., 2021. Geological and Petrological Investigation of the Western North Makran Ophiolites (SE Iran): New Constraints for the Late Jurassic-Cretaceous Tectono-Magmatic and Geodynamic Evolution of the Neo-Tethys Ocean. University of Ferrara, Italy, p. 324.

Barbero, E., Delavari, M., Dolati, A., Saccani, E., Marroni, M., Catanzariti, R., Pandolfi, L., 2020. The Ganj complex reinterpreted as a late cretaceous volcanic arc: Implications for the geodynamic evolution of the North Makran domain (Southeast Iran). J. Asian Earth Sci. 195, 104306.

Barbero, E., Pandolfi, L., Delavari, M., Dolati, A., Saccani, E., Catanzariti, R., Luciani, V., Chiari, M., Marroni, M., 2021a. The western Durkan complex (Makran Accretionary Prism, SE Iran): a late cretaceous tectonically disrupted seamounts chain and its role in controlling deformation style. Geosci. Front. 12, 101106.

Barbero, E., Zaccarini, F., Delavari, M., Dolati, A., Saccani, E., Marroni, M., Pandolfi, L., 2021b. New evidence for late cretaceous plume-related seamounts in the Middle East sector of the Neo-Tethys: Constraints from geochemistry, petrology, and mineral chemistry of the magmatic rocks from the western Durkan complex (Makran Accretionary Prism, SE Iran). Lithos 106228.

Belousov, I., Batanova, V., Sobolev, A., Savelieva, G., Danyushevsky, L., Draayers, E., 2021. Pyroxenites from mantle section of Voykar Ophiolite–Melt/peridotite reaction and crystallization in SSZ mantle. Lithos 388, 106063.

Berly, T.J., Hermann, J., Arculus, R.J., Lapierre, H., 2006. Supra-subduction zone pyroxenites from San Jorge and Santa Isabel (Solomon Islands). J. Petrol. 47, 1531–1555.

Borisova, A.Y., Ceuleneer, G., Kamenetsky, V.S., Arai, S., Béjina, F., Abily, B., Bindeman, I.N., Polvé, M., De Parseval, P., Aigouy, T., 2012. A new view on the petrogenesis of the Oman ophiolite chromitites from microanalyses of chromite-hosted inclusions. J. Petrol. 53, 2411–2440.

Bröcker, M., Omrani, H., Berndt, J., Moslempour, J.M.E., 2021. Unravelling metamorphic ages of suture zone rocks from the Sabzevar and Makran areas (Iran): robust age constraints for the larger Arabia-Eurasian collision zone. J. Metamorph. Geol. 1–31.

Burg, J.-P., 2018. Geology of the onshore Makran accretionary wedge: Synthesis and tectonic interpretation. Earth Sci. Rev. 185, 1210–1231.

Cameron, W.E., 1985. Petrology and origin of primitive lavas from the Troodos ophiolite, cyprus. Contrib. Mineral. Petrol. 89, 239–255.

Choi, S.H., Shervais, J.W., Mukasa, S.B., 2008. Supra-subduction and abyssal mantle peridotites of the Coast Range ophiolite, California: Initiation of Franciscan subduction along a large-offset fracture zone. Geochim. Cosmochim. Acta 72 (A160-A160).

Dick, H.J., Bullen, T., 1984. Chromian spinel as a petrogenetic indicator in abyssal and alpine-type peridotites and spatially associated lavas. Contrib. Mineral. Petrol. 86, 54–76.

Dick, H.J., Natland, J.H., 1996. Late-stage melt evolution and transport in the shallow mantle beneath the East Pacific rise. In: Proceedings-Ocean Drilling Program Scientific Results. National Science Foundation, pp. 103–134.

Downes, H., 2007. Origin and significance of spinel and garnet pyroxenites in the shallow lithospheric mantle: Ultramafic massifs in orogenic belts in Western Europe and NW Africa. Lithos 99, 1–24.

Elthon, D., 1979. High magnesia liquids as the parental magma for ocean floor basalts. Nature 278, 514–518.

Esmaeili, R., Xiao, W., Ebrahimi, M., Zhang, J.E., Zhang, Z., Abd El-Rahman, Y., Han, C., Wan, B., Ao, S., Song, D., 2019. Makran ophiolitic basalts (SE Iran) record late cretaceous Neotethys plume-ridge interaction. Int. Geol. Rev. 1–21.

Falloon, T.J., Meffre, S., Crawford, A.J., Hoernle, K., Hauff, F., Bloomer, S.H., Wright, D.J., 2014. Cretaceous fore-arc basalts from the Tonga arc: Geochemistry and implications for the tectonic history of the SW Pacific. Tectonophysics 630, 21–32.

Gaetani, G.A., Grove, T.L., 1998. The influence of water on melting of mantle peridotite. Contrib. Mineral. Petrol. 131, 323–346.

Garrido, C.J., Bodinier, J.L., Dhuime, B., Bosch, D., Chanefo, I., Bruguier, O., Hussain, S.S., Dawood, H., Burg, J.P., 2007. Origin of the island arc Moho transition zone via melt-rock reaction and its implications for intracrustal differentiation of island arcs: evidence from the Jijal complex (Kohistan complex, northern Pakistan). Geology 35, 683–686.

Ghazi, A.M., Hassanipak, A.A., Mahoney, J.J., Duncan, R.A., 2004. Geochemical characteristics (40)Ar-(39)Ar ages and original tectonic setting of the Band-e-Zeyarat/Dar Anar ophiolite, Makran accretionary prism, SE Iran. Tectonophysics 393, 175–196.

González-Jiménez, J.M., Griffin, W.L., Proenza, J.A., Gervilla, F., O'Reilly, S.Y., Akbulut, M., Pearson, N.J., Arai, S., 2014. Chromitites in ophiolites: how, where, when, why? Part II. The crystallization of chromitites. Lithos 189, 140–158.

Griffin, W.L., Afonso, J.C., Belousova, E.A., Gain, S.E., Gong, X.-H., Gonzalez-Jimenez, J.M., Howell, D., Huang, J.-X., McGowan, N., Pearson, N.J., 2016. Mantle recycling: transition zone metamorphism of Tibetan ophiolitic peridotites and its tectonic implications. J. Petrol. 57, 655–684.

Hawthorne, F.C., Oberti, R., Harlow, G.E., Maresch, W.V., Martin, R.F., Schumacher, J.C., Welch, M.D., 2012. Nomenclature of the amphibole supergroup. Am. Mineral. 97, 2031–2048.

Hellebrand, E., Snow, J.E., Dick, H.J., Hofmann, A.W., 2001. Coupled major and trace elements as indicators of the extent of melting in mid-ocean-ridge peridotites. Nature 410, 677–681.

Henry, H., Tilhac, R., Griffin, W.L., O'Reilly, S.Y., Satsukawa, T., Kaczmarek, M.-A., Grégoire, M., Ceuleneer, G., 2017. Deformation of mantle pyroxenites provides clues to geodynamic processes in subduction zones: Case study of the Cabo Ortegal complex, Spain. Earth Planet. Sci. Lett. 472, 174–185.

Hunziker, D., Burg, J.P., Bouilhol, P., von Quadt, A., 2015. Jurassic rifting at the Eurasian Tethys margin: Geochemical and geochronological constraints from granitoids of

North Makran, southeastern Iran. Tectonics 34, 571–593.
Hunziker, D., Burg, J.P., Moulas, E., Reusser, E., Omrani, J., 2017. Formation and preservation of fresh lawsonite: Geothermobarometry of the North Makran Blueschists, Southeast Iran. J. Metamorph. Geol. 35, 871–895.
Jean, M.M., Shervais, J.W., Choi, S.H., Mukasa, S.B., 2010. Melt extraction and melt refertilization in mantle peridotite of the Coast Range ophiolite: an LA-ICP-MS study. Contrib. Mineral. Petrol. 159, 113–136.
Johan, Z., Martin, R.F., Ettler, V., 2017. Fluids are bound to be involved in the formation of ophiolitic chromite deposits. Eur. J. Mineral. 29, 543–555.
Jung, H., Karato, S.-I., 2001. Water-induced fabric transitions in olivine. Science 293, 1460–1463.
Kamenetsky, V.S., Crawford, A.J., Meffre, S., 2001. Factors controlling chemistry of magmatic spinel: an empirical study of associated olivine, Cr-spinel and melt inclusions from primitive rocks. J. Petrol. 42, 655–671.
Kapsiotis, A., Rassios, A.E., Uysal, I., Grieco, G., Akmaz, R.M., Saka, S., Bussolesi, M., 2018. Compositional fingerprints of chromian spinel from the refractory chrome ores of Metalleion, Othris (Greece): Implications for metallogeny and deformation of chromitites within a "hot" oceanic fault zone. J. Geochem. Explor. 185, 14–32.
Khedr, M.Z., Arai, S., 2016. Chemical variations of mineral inclusions in Neoproterozoic high-Cr chromitites from Egypt: evidence of fluids during chromitite genesis. Lithos 240, 309–326.
Koepke, J., Berndt, J., Horn, I., Fahle, J., Wolff, P., 2014. Partial melting of oceanic gabbro triggered by migrating water-rich fluids: a prime example from the Oman Ophiolite. Geol. Soc. Lond., Spec. Publ. 392, 195–212.
Koga, K.T., Kelemen, P.B., Shimizu, N., 2001. Petrogenesis of the crust-mantle transition zone and the origin of lower crustal wehrlite in the Oman ophiolite. Geochem. Geophys. Geosyst. 2.
Latypov, R., Costin, G., Chistyakova, S., Hunt, E.J., Mukherjee, R., Naldrett, T., 2018. Platinum-bearing chromite layers are caused by pressure reduction during magma ascent. Nat. Commun. 9, 1–7.
McCall, G.J.H., 1997. The geotectonic history of the Makran and adjacent areas of southern Iran. J. Asian Earth Sci. 15, 517–531.
Mccall, G.J.H., 2002. A summary of the geology of the Iranian Makran. In: Tectonic and Climatic Evolution of the Arabian Sea Region, 195, pp. 147–204.
Meshi, A., Boudier, F., Nicolas, A., Milushi, I., 2010. Structure and tectonics of lower crustal and upper mantle rocks in the Jurassic Mirdita ophiolites, Albania. Int. Geol. Rev. 52, 117–141.
Miura, M., Arai, S., Ahmed, A.H., Mizukami, T., Okuno, M., Yamamoto, S., 2012. Podiform chromitite classification revisited: a comparison of discordant and concordant chromitite pods from Wadi Hilti, northern Oman ophiolite. J. Asian Earth Sci. 59, 52–61.
Muroi, R., Arai, S., 2014. Formation process of olivine–clinopyroxene cumulates inferred from Takashima xenoliths, Southwest Japan arc. J. Mineral. Petrol. Sci. 109, 79–84.
Negishi, H., Arai, S., Yurimoto, H., Ito, S., Ishimaru, S., Tamura, A., Akizawa, N., 2013. Sulfide-rich dunite within a thick Moho transition zone of the northern Oman ophiolite: Implications for the origin of Cyprus-type sulfide deposits. Lithos 164, 22–35.
Pandolfi, L., Barbero, E., Marroni, M., Delavari, M., Dolati, A., Di Rosa, M., Frassi, C., Langone, A., Farina, F., MacDonald, C., Saccani, E., 2021. The Bajgan complex revealed as a cretaceous ophiolite-bearing subduction complex: a key to unravel the geodynamics of Makran (Southeast Iran). J. Asian Earth Sci. (In press).
Parkinson, I.J., Pearce, J.A., 1998a. Peridotites from the Izu-Bonin-Mariana forearc (ODP leg 125): evidence for mantle melting and melt-mantle interaction in a supra-subduction zone setting. J. Petrol. 39, 1577–1618.
Parkinson, I.J., Pearce, J.A., 1998b. Peridotites from the Izu–Bonin–Mariana forearc (ODP Leg 125): evidence for mantle melting and melt–mantle interaction in a supra-subduction zone setting. J. Petrol. 39, 1577–1618.
Pearce, J.A., Barker, P., Edwards, S., Parkinson, I.J., Leat, P., 2000a. Geochemistry and tectonic significance of peridotites from the South Sandwich arc–basin system, South Atlantic. Contrib. Mineral. Petrol. 139, 36–53.
Pearce, J.A., Barker, P.F., Edwards, S.J., Parkinson, I.J., Leat, P.T., 2000b. Geochemistry and tectonic significance of peridotites from the South Sandwich arc-basin system, South Atlantic. Contrib. Mineral. Petrol. 139, 36–53.
Qasim Jan, M., Windley, B., 1990. Chromian spinel-silicate chemistry in ultramafic rocks of the Jijal complex, Northwest Pakistan. J. Petrol. 31, 667–715.
Reagan, M.K., Ishizuka, O., Stern, R.J., Kelley, K.A., Ohara, Y., Blichert-Toft, J., Bloomer, S.H., Cash, J., Fryer, P., Hanan, B.B., Hickey-Vargas, R., Ishii, T., Kimura, J.I., Peate, D.W., Rowe, M.C., Woods, M., 2010. Fore-arc basalts and subduction initiation in the Izu-Bonin-Mariana system. Geochem. Geophys. Geosyst. 11.
Reagan, M.K., Pearce, J.A., Petronotis, K., Almeev, R.R., Avery, A.J., Carvallo, C., Chapman, T., Christeson, G.L., Ferre, E.C., Godard, M., Heaton, D.E., Kirchenbaur, M., Kurz, W., Kutterolf, S., Li, H., Li, Y.B., Michibayashi, K., Morgan, S., Nelson, W.R., Prytulak, J., Python, M., Robertson, A.H.F., Ryan, J.G., Sager, W.W., Sakuyama, T., Shervais, J.W., Shimizu, K., Whattam, S.A., 2017. Subduction initiation and ophiolite crust: new insights from IODP drilling. Int. Geol. Rev. 59, 1439–1450.
Ridolfi, F., Renzulli, A., Puerini, M., 2010. Stability and chemical equilibrium of amphibole in calc-alkaline magmas: an overview, new thermobarometric formulations and application to subduction-related volcanoes. Contrib. Mineral. Petrol. 160, 45–66.
Rollinson, H., 2008. The geochemistry of mantle chromitites from the northern part of the Oman ophiolite: inferred parental melt compositions. Contrib. Mineral. Petrol. 156, 273–288.
Rollinson, H., Adetunji, J., 2015. The geochemistry and oxidation state of podiform chromitites from the mantle section of the Oman ophiolite: a review. Gondwana Res. 27, 543–554.
Rospabe, M., Ceuleneer, G., Benoit, M., Abily, B., Pinet, P., 2017. Origin of the dunitic mantle-crust transition zone in the Oman ophiolite: the interplay between percolating magmas and high-temperature hydrous fluids. Geology 45, 471–474.
Rospabe, M., Benoit, M., Ceuleneer, G., Hodel, F., Kaczmarek, M.A., 2018. Extreme geochemical variability through the dunitic transition zone of the Oman ophiolite: Implications for melt/fluid-rock reactions at Moho level beneath oceanic spreading centers. Geochim. Cosmochim. Acta 234, 1–23.
Rospabé, M., Ceuleneer, G., Granier, N., Arai, S., Borisova, A.Y., 2019. Multi-scale development of a stratiform chromite ore body at the base of the dunitic mantle-crust transition zone (Maqsad diapir, Oman ophiolite): the role of repeated melt and fluid influxes. Lithos 350, 105235.
Saccani, E., Tassinari, R., 2015. The Role of MORB and SSZ Magma-Types in the Formation of Jurassic Ultramafic Cumulates in the Mirdita Ophiolites (Albania) as Deduced from Chromian Spinel and Olivine Chemistry.
Saccani, E., Delavari, M., Dolati, A., Marroni, M., Pandolfi, L., Chiari, M., Barbero, E., 2018a. New insights into the geodynamics of Neo-Tethys in the Makran area: evidence from age and petrology of ophiolites from the Coloured Mélange Complex (SE Iran). Gondwana Res. 62, 306–327.
Saccani, E., Dilek, Y., Photiades, A., 2018b. Time-progressive mantle-melt evolution and magma production in a Tethyan marginal sea: a case study of the Albanide-Hellenide ophiolites. Lithosphere 10, 35–53.
Salters, V.J., Stracke, A., 2004. Composition of the depleted mantle. Geochem. Geophys. Geosyst. 5.
Samimi Namin, M., et al., 1983. The 1:250000 Geological Map of Minab, Geological Quadrangle Map of Iran. Geological and Mineral Survey of Iran, Tehran.
Sobolev, A.V., Danyushevsky, L.V., 1994. Petrology and geochemistry of boninites from the north termination of the Tonga Trench - constraints on the generation conditions of primary high-Ca boninite magmas. J. Petrol. 35, 1183–1211.
Spiess, R., Dibona, R., Faccenda, M., Mattioli, M., Renzulli, A., 2017. Mylonitic gabbro nodules of Stromboli (southern Italy): Microstructural evidence of high-temperature deformation of cumulates during the evolution of the magmatic crustal roots of an active volcano. Geol. Soc. Am. Spec. Pap. 526, 89–105.
Stern, R.J., Gerya, T., 2017. Subduction initiation in nature and models: a review. Tectonophysics.
Tamura, A., Arai, S., 2006. Harzburgite-dunite-orthopyroxenite suite as a record of supra-subduction zone setting for the Oman ophiolite mantle. Lithos 90, 43–56.
Tamura, A., Morishita, T., Ishimaru, S., Arai, S., 2014. Geochemistry of spinel-hosted amphibole inclusions in abyssal peridotite: Insight into secondary melt formation in melt-peridotite reaction. Contrib. Mineral. Petrol. 167.
Tilhac, R., Gregoire, M., O'Reilly, S.Y., Griffin, W.L., Henry, H., Ceuleneer, G., 2017. Sources and timing of pyroxenite formation in the sub-arc mantle: Case study of the Cabo Ortegal complex, Spain. Earth Planet. Sci. Lett. 474, 490–502.
Zagrtdenov, N.R., Ceuleneer, G., Rospabe, M., Borisova, A.Y., Toplis, M.J., Benoit, M., Abily, B., 2018. Anatomy of a chromitite dyke in the mantle/crust transition zone of the Oman ophiolite. Lithos 312, 343–357.